Globally Asymptotically Stable Sensor-Based Simultaneous Localization and Mapping

Bruno J. N. Guerreiro, *Member, IEEE*, Pedro Batista, *Member, IEEE*, Carlos Silvestre, *Member, IEEE*, and Paulo Oliveira, *Senior Member, IEEE*

***Abstract*—This paper presents the design, analysis, and experimental validation of a globally asymptotically stable (GAS) filter for simultaneous localization and mapping (SLAM), with application to unmanned aerial vehicles. The SLAM problem is formulated in a sensor-based framework and modified in such a way that the underlying system structure can be regarded as linear time varying for observability analysis and filter design purposes, from which a linear Kalman filter with GAS error dynamics follows naturally. The performance and consistency validation of the proposed sensor-based SLAM filter are successfully assessed with real data, acquired indoors, using an instrumented quadrotor.**

***Index Terms*—Aerial robotics, globally asymptotically stable (GAS), mapping, sensor fusion, simultaneous localization and mapping (SLAM).**

I. Introduction

RELIABLE navigation and positioning of unmanned aerial vehicles (UAVs) are fundamental for any autonomous mission, particularly in unknown environments where absolute positioning systems are absent or unreliable. The motivation for this study arises from the usage of autonomous rotorcraft for automatic inspection of critical infrastructures and buildings, such as bridges, electric power lines, dams, construction areas, etc. Near these structures, the global positioning system signal may be unreliable or nonexistent, whereas the electromagnetic interference and the existence of ferromagnetic materials may degrade any magnetometer measurement to the point of becoming unusable. This is of special importance as these dynamically unstable vehicles have to work as close as possible to the inspection target. The use of aided navigation techniques, as proposed in this study using a simultaneous localization and mapping (SLAM) algorithm, aims to solve this problem in such a way that these sensors are made redundant.

Over the past decades, the research community has devoted tremendous effort in the field of probabilistic SLAM. The seminal works that established the statistical foundations to describe the relationships between landmarks and their correlations include [1]–[3]. Further research showed that a full and consistent solution to this problem would require all the vehicle pose and map variables to be considered in a single, and potentially large, state vector. This requirement made the problem intrinsically nonlinear and one of the technical solutions that emerged from this challenge was to use the much celebrated extended Kalman filter (EKF) [4], [5]. For a detailed survey and tutorial on SLAM, see [6]–[8], and references therein, which include a significant number of successful implementations of SLAM algorithms in real-world scenarios. The association of measured and state landmarks is one of the major sources of inconsistency in SLAM algorithms and considerable effort has been put into this issue. Several strategies have emerged, namely, simplistic nearest neighbor validation gating, joint compatibility branch and bound (JCBB) [9], combined constrained data association [10], and other strategies, such as multihypothesis data association or particle filters, that imply changes or a different algorithm.

A general proof of global convergence for the EKF, to the best of the authors' knowledge, is yet to be found. Nonetheless, there are some notable SLAM convergence results [11], [12], which usually assume that the linearized system matrices are evaluated at the ideal values of the state variables. This linearization may lead to inconsistency as it was first pointed out in [13], and subsequently, acknowledged and discussed in [12], [14], and [15]. In order to minimize the inconsistency problems induced by the linearization, some algorithms have been proposed, such as the robocentric map joining algorithm [16], or the first-estimates Jacobian EKF [17]. The robocentric map joining approach bears resemblance to the method proposed in this paper, in the sense that the filtering process takes place in the sensor or vehicle coordinate space. In [18], Bishop and Jensfelt resort to stochastic stability concepts to provide results concerning the boundedness and convergence of the expected estimation error of an EKF-based polar SLAM for a unicycle model in the presence of noise, when there is access to both linear and angular velocity measurements.

The contribution of this paper is the design, analysis, and experimental validation of a novel 2-D sensor-based SLAM

Manuscript received September 22, 2012; revised April 9, 2013; accepted July 3, 2013. Date of publication September 25, 2013; date of current version December 2, 2013. This paper was recommended for publication by Associate Editor P. Jensfelt and Editor D. Fox upon evaluation of the reviewers' comments. This work was supported in part by the Project FCT (PEst-OE/EEI/LA0009/2011), by the Project FCT AMMAIA (PTDC/HIS-ARQ/103227/2008), and by the Project AIRTICI from AdI through the POS Conhecimento Program that includes FEDER funds. The work of B. J. N. Guerreiro was supported by the Ph.D. Student Grant SFRH/BD/21781/2005 from the Portuguese FCT POCTI programme.

B. J. N. Guerreiro, P. Batista, and P. Oliveira are with the Institute for Systems and Robotics, Instituto Superior Técnico, Technical University of Lisbon, Lisbon 1049 001, Portugal (e-mail: bguerreiro@isr.ist.utl.pt; pbatista@isr.ist.utl.pt; pjcro@isr.ist.utl.pt).

C. Silvestre is with the Institute for Systems and Robotics, Instituto Superior Técnico, Technical University of Lisbon, Lisbon 1049 001, Portugal and also with the Faculty of Science and Technology, University of Macau, Taipa, Macau (e-mail: cjs@isr.ist.utl.pt)

Color versions of one or more of the figures in this paper are available online at http://ieeexplore.ieee.org.

Digital Object Identifier 10.1109/TRO.2013.2273838

1552-3098 © 2013 IEEE

Fig. 1. Instrumented quadrotor.

filter, which can be used in structured 3-D environments if the altitude is included in the system dynamics, as part of an integrated SLAM algorithm, that: 1) has globally asymptotically stable error dynamics; 2) resorts to the linear and angular motion kinematics, which are exact; 3) can be generalized into full 3-D SLAM, if 3-D landmarks are available; 4) builds on the well-established linear time-varying (LTV) Kalman filtering theory; 5) explicitly estimates the rate gyro bias, merging low-bandwidth landmark observations with high-bandwidth rate gyro measurements; and 6) is validated in terms of performance and consistency, using real data, acquired using an instrumented quadrotor, shown in Fig. 1. The result of this filter is the solution of the SLAM problem in the vehicle frame, where the vehicle pose is deterministic, as it is simply that of the vehicle frame, and the positions of the landmarks rotate and translate according to the vehicle motion, in a similar fashion to what happens in [16]. An essential feature of the proposed filter is the modification of the nominal nonlinear system dynamics such that it can be regarded as LTV for observability and convergence analysis purposes, even though it still is intrinsically nonlinear. Conversely, the system dynamics described in [16] include the full odometry of the vehicle in the state vector, rendering the use of the observability analysis strategy proposed hereafter nontrivial. It must also be stressed that the system dynamics used in the design and analysis of the proposed Kalman filter are exact and no approximations or linearizations are performed. The proposed solution builds on previous sensor-based navigation filters that are proposed in [19]–[21]. Regarding the work presented in [18], the main contribution of this paper is that the observability results are global and constructive, in the sense that both necessary and sufficient conditions for observability are derived, with clear physical interpretation, and a system structure naturally appears for observer design purposes, yielding globally asymptotically stable error dynamics. Furthermore, the proposed formulation enables the solution of the SLAM problem even in the absence of linear velocity measurements, which are not usually available for aerial platforms. If available, these measurements could be used in the proposed filter to further improve the quality of the obtained estimates. A map described in an Earth-fixed reference frame can also be obtained by including unobservable position and direction landmarks that represent the reference frame in the sensor-based frame or, alternatively, by formulating an algorithm under the scope of the extended Procrustes problem, as detailed in the preliminary work presented in [22].

A. Paper Structure and Notation

The paper is organized as follows. Section II introduces the problem at hand, including the sensor-based paradigm and the nominal system dynamics. A constructive observability analysis is carried out in Section III and Section IV details the design of the sensor-based SLAM filter. The experimental results using an instrumented quadrotor platform are presented and discussed in Section V. Finally, the conclusions and directions of future work are provided in Section VI. A preliminary version of this study can be found in [22] and [23]. In addition to the detailed derivation and discussion of those results, this paper presents necessary and sufficient observability conditions, for position-only landmarks and for position and direction landmarks. Moreover, a loop-closure algorithm is implemented for an improved consistency validation of the proposed algorithms.

Throughout the paper, the symbol $\mathbf{0}_{n\times m}$ denotes an $n \times m$ matrix of zeros, $\mathbf{I}_n$ an identity matrix with dimension $n \times n$, and $\mathrm{diag}(\mathbf{A}_1, \ldots, \mathbf{A}_n)$ a block diagonal matrix. When the dimensions are omitted the matrices are assumed to be of appropriate dimensions. For some $\mathbf{a}, \mathbf{b} \in \mathbb{R}^3$, $\mathbf{S}(\mathbf{a})$ is the 3-D skew-symmetric matrix such that $\mathbf{S}(\mathbf{a})\mathbf{b}$ is the cross product $\mathbf{a} \times \mathbf{b}$, and for some $a \in \mathbb{R}$, $\mathbf{S}(a)$ denotes the 2-D skew-symmetric matrix $\mathbf{S}(a) = \begin{bmatrix} 0 & -a \\ a & 0 \end{bmatrix}$.

II. Problem Statement

The traditional EKF-based SLAM filtering solution models the estimated features and vehicle pose in an absolute coordinate frame, usually denoted as the Earth-fixed reference frame, while the measurements are obtained in body-fixed coordinates, i.e., in the frame rigidly attached to the vehicle. Even in the 2-D space, the dynamic equations of this system require a representation of the attitude of the vehicle to transform each measured landmark from the sensor space into the reference frame using, for instance, rotation matrices, quaternions, or Euler angles. Thus, the system equations are usually linearized to compute the state pseudo-covariance matrix, potentially resulting in inconsistency or even failure of the SLAM filter, as pointed out in [13] and [15], mainly when the linearization condition is systematically far from the actual attitude of the vehicle. Moreover, the employment of attitude representations necessarily carries pitfalls such as singularities, topological limitations to achieve continuous global stabilization, double covering, slow convergence near unstable equilibrium points, or unwinding phenomena, depending on the parameterization, as detailed in [24] and [25]. A remarkable and successful effort to reduce the inconsistency related to these linearizations was proposed in [16], with the redefinition of the SLAM dynamics in a vehicle-centered representation,

which was shown to have better consistency properties both in simulated and real-world environments. Nonetheless, this approach still considers the estimation of the incremental vehicle pose (driven by the odometry) by including these variables in the state vector. The Earth-fixed reference frame is also included in the mentioned work as an unobservable state, which is integrated in open loop using odometry estimates of the vehicle motion, and is used afterwards to transform the map and vehicle trajectory back into the reference frame.

The concept of the sensor-based SLAM approach that is presented in this paper is the design of the filter directly in the space of the sensors, taking into account the original noise characteristics of each sensor. At each instant, the vehicle can localize itself trivially, at the origin of the robocentric frame, and have a local representation of the environment map using landmarks. Nonetheless, the filter avoids the use of any representation of the pose of the vehicle both in the measurement equation and in the state equations concerning the representation of the environment. Using techniques similar to [22], the full pose of the vehicle in the Earth-fixed frame can also be computed at each sampling instant, by using exclusively the history of the sensor-based map of the environment. It is noted that the proposed technique is in line with, and complements, the so-called sensor-based control paradigm, as the quantities in the sensor frame, required for control purposes, are readily estimated by the filter presented in the sequel.

A. Nominal Nonlinear System Dynamics

Let E denote the Earth-fixed reference frame, B the body-fixed frame, and ${}^{E}_{B}\mathbf{R}(t) \in \mathrm{SO}(3)$ the rotation matrix from B to E. Let also ${}^{E}\mathbf{p}_{B}(t) \in \mathbb{R}^3$ denote the position of the origin of B, described in E, and $\mathbf{v}_{B}(t) \in \mathbb{R}^3$ the velocity of the vehicle relative to E, expressed in B. The linear and angular motion kinematics of the vehicle are given by

$$\begin{cases} {}^{E}\dot{\mathbf{p}}_{B}(t) = {}^{E}_{B}\mathbf{R}(t)\,\mathbf{v}_{B}(t) \\ {}^{E}_{B}\dot{\mathbf{R}}(t) = {}^{E}_{B}\mathbf{R}(t)\,\mathbf{S}[\boldsymbol{\omega}_{B}(t)] \end{cases}$$

where $\boldsymbol{\omega}_{B}(t) \in \mathbb{R}^3$ is the angular velocity of the vehicle relative to E, expressed in B. Consider also the ZYX-Euler angles which can be used to decompose the rotation matrix ${}^{E}_{B}\mathbf{R}(t)$ as ${}^{E}_{B}\mathbf{R}(t) = \mathbf{R}_{z}(\psi(t))\,\mathbf{R}_{y}(\theta(t))\,\mathbf{R}_{x}(\phi(t))$, where $\phi(t), \theta(t)$, and $\psi(t)$ denote the roll, pitch, and yaw angles, respectively, whereas $\mathbf{R}_{x}(.)$, $\mathbf{R}_{y}(.)$, and $\mathbf{R}_{z}(.)$ denote the rotation matrices about the x-, y-, and z-axes, respectively.

Assuming that an inertial measurement unit (IMU) is aligned with B, the rate gyros provide angular velocity measurements, $\boldsymbol{\omega}_{B_g}(t) \in \mathbb{R}^3$, corrupted with bias and noise, as given by

$$\boldsymbol{\omega}_{B_g}(t) = \boldsymbol{\omega}_{B}(t) + \mathbf{b}_{\omega}(t) + \mathbf{n}_{\omega}(t)$$

where $\mathbf{b}_{\omega}(t) \in \mathbb{R}^3$ denotes the bias of the triaxial rate gyro, which is slowly time varying, and $\mathbf{n}_{\omega}(t) \in \mathbb{R}^3$ corresponds to the rate gyro noise. As the rate gyro measurements will be used in the system dynamics, the estimation of the measurement bias will be of paramount importance for the consistency of the filter. Using standard filtering techniques (see for instance [26] and references therein), the roll and pitch angles can be obtained using only rate gyros and accelerometer measurements, enabling the definition of a horizontal body-fixed frame H, such that ${}^{E}\mathbf{p}_{H}(t) = {}^{E}\mathbf{p}_{B}(t)$ denotes the position of frame H described in frame E, ${}^{E}_{H}\mathbf{R}(t) = \mathbf{R}_{z}(\psi(t))$ the rotation from frame H to frame E, and ${}^{H}_{B}\mathbf{R}(t) = \mathbf{R}_{y}(\theta(t))\,\mathbf{R}_{x}(\phi(t))$ the rotation from B to H.

Using the rotation matrix ${}^{H}_{B}\mathbf{R}(t)$ and the known pose configuration of the sensor relative to frame B, the measurements of a laser scanner mounted horizontally in the vehicle can be projected into H and the respective measurement noise covariance matrix can account for the estimation errors of ${}^{H}_{B}\mathbf{R}(t)$. In this way, the laser measurements represent a horizontal profile of the environment, from which the position of the vehicle and a map of the environment in 2-D can be obtained using a SLAM algorithm. The underlying assumption is that the environment is fairly structured along the vertical direction, that is, with limited variation of features for different altitudes, which include indoor environments, outdoor fields with trees, piers, or conventional buildings. It is also assumed that the vehicle is not too close to the lower and upper boundaries of the environment, which inside a building would translate into neither being too close to the ground nor too close to the ceiling. As the SLAM algorithm herewith derived provides a 2-D position and map independently of the altitude position, for the sake of clarity and with a slight abuse of notation, it is considered in the remainder of this paper that all vectors are in 2-D and all rotation matrices belong to SO(2), unless otherwise stated.

Consider that each landmark that is detected can be represented by a 2-D position and some auxiliary characteristics depending on the type of feature. For instance, a wall corner can be represented by the position of the edge and two line segments, providing not only a position measurement but also one or two direction readings. Considering the case of just a single direction associated with a landmark, the position and the direction associated with the ith landmark in H, denoted, respectively, by $\mathbf{p}_{i}(t) \in \mathbb{R}^2$ and $\mathbf{d}_{i}(t) \in \mathbb{R}^2$, satisfy

$$\begin{cases} \mathbf{p}_{i}(t) = {}^{E}_{H}\mathbf{R}^{T}(t)\,({}^{E}\mathbf{p}_{i} - {}^{E}\mathbf{p}_{H}(t)) \\ \mathbf{d}_{i}(t) = {}^{E}_{H}\mathbf{R}^{T}(t)\,{}^{E}\mathbf{d}_{i} \end{cases}$$

where ${}^{E}\mathbf{p}_{i} \in \mathbb{R}^2$ and ${}^{E}\mathbf{d}_{i} \in \mathbb{R}^2$ denote the 2-D position and direction associated with the landmark, respectively, described in the reference frame E and considered to be static. In the sensor-based framework, their kinematics can be written as

$$\begin{cases} \dot{\mathbf{p}}_{i}(t) = -\left[r_{g}(t) - b_{r}(t)\right]\,\mathbf{S}\,\mathbf{p}_{i}(t) - \mathbf{v}(t) \\ \dot{\mathbf{d}}_{i}(t) = -\left[r_{g}(t) - b_{r}(t)\right]\,\mathbf{S}\,\mathbf{d}_{i}(t) \end{cases} \tag{1}$$

where $\mathbf{S} := \mathbf{S}(1)$, $r_{g}(t) \in \mathbb{R}$ is the z-component of rate gyro measurement expressed in H, $b_{r}(t) \in \mathbb{R}$ is the corresponding rate gyro bias, and $\mathbf{v}(t) \in \mathbb{R}^2$ denotes the linear velocity of the vehicle relative to E, expressed in H. These equations describe the linear and angular motion kinematics for each landmark, which are exact. It is also noted that, because the bias term is expressed in H, it is not constant. Instead, its derivative depends on the roll, pitch, and respective angular velocities, which can all be obtained using a complementary filter with globally asymptotically stable error dynamics based on the acceleration and

rate gyro readings; see [26] for details. In the remainder of the paper, it is considered, without loss of generality for observer design purposes, $\dot{b}_r(t) = 0$. In the final design, an additional input is naturally considered to model the exact bias dynamics.

In a SLAM state-space formulation, the full state vector, here denoted as $\mathbf{x}_F(t) \in \mathbb{R}^{n_F}$, can be decomposed into vehicle specific variables $\mathbf{x}_V(t) \in \mathbb{R}^{n_V}$, and landmark variables $\mathbf{x}_M(t) \in \mathbb{R}^{n_M}$. In the proposed formulation, the vehicle state vector is composed by the horizontal linear velocity, $\mathbf{v}(t) \in \mathbb{R}^2$, and the angular velocity bias, $b_r(t) \in \mathbb{R}$, all described in H, yielding $\mathbf{x}_V(t) = [\,\mathbf{v}^T(t) \quad b_r(t)\,]^T$. Notice that this vehicle state vector does not consider any information about the position and attitude of the vehicle relative to the reference frame.

Each landmark vector, denoted as $\mathbf{x}_i(t) \in \mathbb{R}^{n_i}$, can feature the position of a landmark and up to two directions, e.g., to represent a corner landmark it would be $\mathbf{x}_i(t) = [\,\mathbf{p}_i^T(t) \quad \mathbf{d}_{a_i}^T(t) \quad \mathbf{d}_{b_i}^T(t)\,]^T$. The set of landmarks, $\mathcal{I}$, considered in the state vector can be arranged in such a way that the first m landmarks denote the ones that are visible/observed and the next p are the nonvisible/unobserved landmarks, respectively, $\mathcal{I}_O = \{1, \ldots, m\}$ and $\mathcal{I}_U = \{m+1, \ldots, m+p\}$, yielding a natural decomposition of the landmark state vector such that $\mathbf{x}_M(t) = [\,\mathbf{x}_O^T(t) \quad \mathbf{x}_U^T(t)\,]^T$, where $\mathbf{x}_O(t) = \{\mathbf{x}_i(t)\} \in \mathbb{R}^{n_O}$ for all $i \in \mathcal{I}_O$, and $\mathbf{x}_U(t) = \{\mathbf{x}_i(t)\} \in \mathbb{R}^{n_U}$ for all $i \in \mathcal{I}_U$.

With the aforementioned introduction and considering that the linear velocity and the rate gyro bias are slowly time varying, the complete system dynamics in H can now be written as

$$\begin{cases} \dot{\mathbf{x}}_V(t) = \mathbf{0} \\ \dot{\mathbf{x}}_i(t) = \mathbf{A}_{MV_i}(\mathbf{x}_i(t))\,\mathbf{x}_V(t) + \mathbf{A}_{M_i}(t)\,\mathbf{x}_i(t) \;\forall_{i\in\mathcal{I}} \\ \mathbf{y}_i(t) = \mathbf{x}_i(t) \;\; \forall_{i\in\mathcal{I}_O} \end{cases} \tag{2}$$

where considering landmarks with only one direction, it is a matter of algebraic manipulation to obtain

$$\mathbf{A}_{MV_i}(\mathbf{x}_i(t)) = \begin{bmatrix} -\mathbf{I}_2 & \mathbf{S}\,\mathbf{p}_i(t) \\ \mathbf{0}_{2\times 2} & \mathbf{S}\,\mathbf{d}_i(t) \end{bmatrix}$$

and $\mathbf{A}_{M_i}(t) = -r_g(t)\,\mathbf{S}_2$, denoting $\mathbf{S}_n$ as the block diagonal matrix formed using n times the matrix $\mathbf{S}$, in this case $\mathbf{S}_2 = \mathrm{diag}\,(\mathbf{S}, \mathbf{S})$. For the case where there are two directions associated with the ith landmark, the aforementioned matrices would be defined as $\mathbf{A}_{M_i}(t) = -r_g(t)\,\mathbf{S}_3$ and

$$\mathbf{A}_{MV_i}(\mathbf{x}_i(t)) = \begin{bmatrix} -\mathbf{I}_2 & \mathbf{S}\,\mathbf{p}_i(t) \\ \mathbf{0}_{2\times 2} & \mathbf{S}\,\mathbf{d}_{a_i}(t) \\ \mathbf{0}_{2\times 2} & \mathbf{S}\,\mathbf{d}_{b_i}(t) \end{bmatrix}.$$

The nominal system dynamics (2) assumes that the vehicle has a constant linear velocity and that the angular velocity measurement bias is also constant. However, by opening the filter tolerance to model uncertainty, using higher disturbance noise covariances, it is possible to track these slowly time-varying variables.

B. Problem Statement

The problem considered in this paper is that of designing a filter with globally asymptotically stable error dynamics for the nominal nonlinear system (2), considering also additive system disturbances and sensor noise. Sections III and IV are intended to tackle this problem, presenting the observability analysis, convergence properties, and the SLAM filter design.

III. Observability Analysis

The main focus of this section is to obtain the necessary and sufficient conditions for the observability of the proposed formulation of the SLAM problem, with a clear physical interpretation. In addition, the analysis is constructive in the sense that a Kalman filter can be readily applied, identifying the nonlinear system with a particular LTV system, yielding globally asymptotically stable error dynamics. The observability analysis considered in this study is deterministic, as the dynamic model is considered noise free for analysis purposes. Nonetheless, the experimental results presented in Section V provide evidence that the system is, indeed, convergent in the presence of noise. This approach has been successfully applied in the past by the authors, for instance in [27].

For observability and filter design purposes, the nonvisible features are not considered, as they are simply propagated in open loop and are evidently unobservable. However, the observability analysis presented in this study shows that this fact has no influence in the observability and convergence of both the visible landmarks and the variables related with the vehicle dynamics, $\mathbf{v}$ and b_r. Discarding the nonvisible landmarks, the reduced state vector is $\mathbf{x}(t) = [\,\mathbf{x}_V^T(t) \quad \mathbf{x}_O^T(t)\,]^T \in \mathbb{R}^{n_x}$, recalling that $\mathbf{x}_O(t) = [\,\mathbf{x}_1^T(t) \quad \cdots \quad \mathbf{x}_m^T(t)\,]^T \in \mathbb{R}^{n_O}$ denotes the vector of visible landmarks, whereas the output vector is $\mathbf{y}(t) = [\,\mathbf{y}_1^T(t) \quad \cdots \quad \mathbf{y}_m^T(t)\,]^T \in \mathbb{R}^{n_y}$, with each landmark output given by $\mathbf{y}_i(t) = [\,\mathbf{y}_{p_i}^T(t) \quad \mathbf{y}_{d_i}^T(t)\,]^T$ for a position landmark with one associated direction. Thus, it is possible to rewrite the nominal nonlinear system (2) as

$$\begin{cases} \dot{\mathbf{x}}(t) = \mathbf{A}(t, \mathbf{x}_O(t))\,\mathbf{x}(t) \\ \mathbf{y}(t) = \mathbf{C}\,\mathbf{x}(t) \end{cases} \tag{3}$$

where

$$\mathbf{A}(t, \mathbf{x}_O(t)) := \begin{bmatrix} \mathbf{0}_{n_V\times n_V} & \mathbf{0}_{n_V\times n_O} \\ \mathbf{A}_{MV}(\mathbf{x}_O(t)) & \mathbf{A}_M(t) \end{bmatrix} \in \mathbb{R}^{n_x\times n_x}$$

$$\mathbf{A}_M(t) := \mathrm{diag}\,(\mathbf{A}_{M_1}(t), \ldots, \mathbf{A}_{M_m}(t)) \in \mathbb{R}^{n_O\times n_O}$$

$$\mathbf{A}_{MV}(\mathbf{x}_O(t)) := [\,\mathbf{A}_{MV_1}^T(\mathbf{x}_1(t)) \;\ldots\; \mathbf{A}_{MV_m}^T(\mathbf{x}_m(t))\,]^T$$

and $\mathbf{C} := [\,\mathbf{0}_{n_O\times n_V} \quad \mathbf{I}_{n_O}\,] \in \mathbb{R}^{n_O\times n_x}$. Consider the previous nonlinear system rewritten as

$$\begin{cases} \dot{\mathbf{x}}(t) = \mathbf{A}(t, \mathbf{y}(t))\,\mathbf{x}(t) \\ \mathbf{y}(t) = \mathbf{C}\,\mathbf{x}(t). \end{cases} \tag{4}$$

Assuming that the output signal $\mathbf{y}(t)$ is known for all $t \geq t_0$, it can be seen that this dynamic system can be regarded as a LTV system, even though it still is, in fact, a nonlinear system. As the system matrix $\mathbf{A}(t, \mathbf{y}(t))$ depends on the system output, $\mathbf{y}(t)$, it can be considered a time-varying matrix, $\mathbf{A}(t) = \mathbf{A}(t, \mathbf{y}(t))$.

However, this is not a problem for observability analysis and observer design purposes, as the output is available and can be considered a known function of t. The same approach has been pursued in [27], where further details on preliminary results can be found. In the remainder of this analysis, when referring to the *nonlinear system* (4) *regarded as LTV*, or in short, the *LTV system* (4), it is implied that the output signal is considered a known function of t, and thus, the system matrix $\mathbf{A}(t, \mathbf{y}(t))$ is also a known matrix function of t.

In order to simplify the analysis, let $\mathbf{R}_g(t) \in \mathrm{SO}(2)$ be a rotation matrix such that $\dot{\mathbf{R}}_g(t) = r_g(t)\mathbf{R}_g(t)\mathbf{S}$ and consider the Lyapunov state transformation [28], $\mathbf{z}(t) := \mathbf{T}(t)\mathbf{x}(t)$, which preserves stability and observability properties, with

$$\mathbf{T}(t) = \mathrm{diag}\left(\mathbf{I}_{n_V}, \mathbf{T}_M(t)\right)$$
$$\mathbf{T}_M(t) = \mathrm{diag}\left(\mathbf{T}_1(t), \ldots, \mathbf{T}_m(t)\right)$$

and $\mathbf{T}_i(t) = \mathrm{diag}\left(\mathbf{R}_g(t), \mathbf{R}_g(t)\right) \in \mathbb{R}^{n_i \times n_i}$, with $n_i = 4$, considering a position landmark with one associated direction. It is a matter of computation to show that the new nonlinear system is given by

$$\begin{cases} \dot{\mathbf{z}}(t) = \boldsymbol{\mathcal{A}}(t, \mathbf{x}_O(t))\,\mathbf{z}(t) \\ \mathbf{y}(t) = \boldsymbol{\mathcal{C}}(t)\,\mathbf{z}(t) \end{cases} \tag{5}$$

which can also be rewritten as

$$\begin{cases} \dot{\mathbf{z}}(t) = \boldsymbol{\mathcal{A}}(t, \mathbf{y}(t))\,\mathbf{z}(t) \\ \mathbf{y}(t) = \boldsymbol{\mathcal{C}}(t)\,\mathbf{z}(t) \end{cases} \tag{6}$$

where

$$\boldsymbol{\mathcal{A}}(t, \mathbf{y}(t)) = \begin{bmatrix} \mathbf{0}_{n_V \times n_V} & \mathbf{0}_{n_V \times n_O} \\ \boldsymbol{\mathcal{A}}_{MV}(\mathbf{y}(t)) & \mathbf{0}_{n_O \times n_O} \end{bmatrix} \in \mathbb{R}^{n_x \times n_x}$$
$$\boldsymbol{\mathcal{A}}_{MV}(\mathbf{y}(t)) = \left[\, \boldsymbol{\mathcal{A}}^T_{MV_1}(\mathbf{y}_1(t)) \quad \ldots \quad \boldsymbol{\mathcal{A}}^T_{MV_m}(\mathbf{y}_m(t)) \,\right]^T$$
$$\boldsymbol{\mathcal{A}}_{MV_i}(\mathbf{y}_i(t)) = \begin{bmatrix} -\mathbf{R}_g(t) & \mathbf{R}_g(t)\mathbf{S}\,\mathbf{y}_{p_i}(t) \\ \mathbf{0}_{2\times 2} & \mathbf{R}_g(t)\mathbf{S}\,\mathbf{y}_{d_i}(t) \end{bmatrix}$$

and $\boldsymbol{\mathcal{C}}(t) = \mathbf{C}\,\mathbf{T}^T(t)$. The following lemma provides the basis for the observability analysis of this type of systems.

Lemma 1 ([27, Lemma 1]): Given the system output $\mathbf{y}(t)$ for all $t \in \mathcal{T} = [t_0, t_f]$, if the observability Gramian $\boldsymbol{\mathcal{W}}(t_0, t_f)$ associated with the pair $(\boldsymbol{\mathcal{A}}(t, \mathbf{y}(t)), \boldsymbol{\mathcal{C}}(t))$ on $\mathcal{T}$ is invertible, then system (6) is observable on $\mathcal{T}$, in the sense that the initial condition $\mathbf{z}(t_0)$ is uniquely defined.

The first result presented in this study establishes sufficient conditions for observability of the nonlinear system (4), regarded as LTV. The remainder of the observability analysis will follow by establishing that a GAS observer for the system (4) regarded as LTV is also a GAS observer for the nominal nonlinear system, which enables the design of such an observer considering only the system regarded as LTV. Furthermore, it is also shown that the proposed conditions for observability are both sufficient and necessary, and that the system regarded as LTV is uniformly completely observable (UCO). This last result is the foundation of the design of the proposed GAS observer.

Prior to the first result, a realistic assumption about the detected landmarks is presented, which basically states that all detected position landmarks are different and have nonzero norm, and that any direction also has nonzero norm. This is the case when using a laser scanner, since the origin is the laser firing point and it is impossible to have two laser points of the same scan with exactly the same bearing.

Assumption 1: For any detected landmark $i \in \mathcal{I}_O$, its position and any associated direction satisfies $\mathbf{y}_{p_i}(t) \neq \mathbf{0}$ and $\mathbf{y}_{d_i}(t) \neq \mathbf{0}$ for all $t \geq t_0$. Furthermore, any two detected position landmarks $i, j, \in \mathcal{I}_O$, with $i \neq j$, satisfy $\mathbf{y}_{p_i}(t) \neq \mathbf{y}_{p_j}(t)$ for all $t \geq t_0$.

Theorem 2: Suppose that Assumption 1 holds. Then, the nonlinear system (4) regarded as LTV is observable on $\mathcal{T} := [t_0, t_f]$, in the sense that, given the system output, the initial condition is uniquely defined, if there exists a time instant $t_1 \in \mathcal{T}$ such that there exist, at least, either

1) two visible position landmarks, $\mathbf{y}_{p_1}(t_1)$ and $\mathbf{y}_{p_2}(t_1)$ or
2) one visible position landmark $\mathbf{y}_{p_1}(t_1)$ with, at least, one associated direction $\mathbf{y}_{d_1}(t_1)$ or
3) one visible position landmark $\mathbf{y}_{p_1}(t_1)$ with nonzero derivative, $\dot{\mathbf{y}}_{p_1}(t_1) \neq \mathbf{0}$.

Proof: As the Lyapunov transformation $\mathbf{T}(t)$ preserves observability, this proof establishes sufficient conditions of observability for the nonlinear system (6) regarded as LTV, which are also valid for the nominal nonlinear system (4), also regarded as LTV. Using Lemma 1, system (6), regarded as LTV, is observable on $\mathcal{T}$ if the observability Gramian associated with the pair $(\boldsymbol{\mathcal{A}}(t, \mathbf{y}(t)), \boldsymbol{\mathcal{C}}(t))$ on $\mathcal{T}$ is invertible. The proof follows by establishing that this is the case. Considering that every landmark has an associated direction, the transition matrix associated with $\boldsymbol{\mathcal{A}}(t, \mathbf{y}(t))$ is given by

$$\boldsymbol{\phi}(t, t_0) = \begin{bmatrix} \mathbf{I}_{n_V} & \mathbf{0} \\ \boldsymbol{\phi}_{MV}(t, t_0) & \mathbf{I}_{n_O} \end{bmatrix}$$

where

$$\boldsymbol{\phi}_{MV}(t, t_0) = \left[\, \boldsymbol{\phi}^T_{MV_1}(t, t_0) \quad \cdots \quad \boldsymbol{\phi}^T_{MV_m}(t, t_0) \,\right]^T$$
$$\boldsymbol{\phi}_{MV_i}(t, t_0) = \int_{t_0}^{t} \mathbf{T}_i(\sigma)\,\mathbf{F}_i(\sigma)\,d\sigma$$

and

$$\mathbf{F}_i(\sigma) = \begin{bmatrix} -\mathbf{I}_2 & \mathbf{S}\,\mathbf{y}_{p_i}(\sigma) \\ \mathbf{0}_{2\times 2} & \mathbf{S}\,\mathbf{y}_{d_i}(\sigma) \end{bmatrix}.$$

Consider the vector $\mathbf{c} := \left[\mathbf{c}_V^T \;\; \mathbf{c}_M^T\right]^T \in \mathbb{R}^{n_x}$, where $\mathbf{c}_V := \left[\mathbf{c}_v^T \;\; c_b\right]^T$, $\mathbf{c}_M := \left[\mathbf{c}_1^T \;\ldots\; \mathbf{c}_m^T\right]^T$, $c_b \in \mathbb{R}$, $\mathbf{c}_v \in \mathbb{R}^2$, and $\mathbf{c}_i = [\mathbf{c}_{p_i}^T \quad \mathbf{c}_{d_i}^T]^T$, with $\mathbf{c}_{p_i}, \mathbf{c}_{d_i} \in \mathbb{R}^2$. If $\boldsymbol{\mathcal{W}}(t_0, t_f)$ denotes the observability Gramian associated with the pair $(\boldsymbol{\mathcal{A}}(t, \mathbf{y}(t)), \boldsymbol{\mathcal{C}}(t))$ on $[t_0, t_f]$, it is a matter of computation to show that

$$\mathbf{c}^T \boldsymbol{\mathcal{W}}(t_0, t_f)\,\mathbf{c} = \int_{t_0}^{t_f} \left\|\mathbf{f}(t_0, \tau)\right\|^2 d\tau$$

where

$$\mathbf{f}(t_0, \tau) = \mathbf{c}_M + \int_{t_0}^{\tau} \mathbf{T}_M(\sigma)\,\mathbf{F}(\sigma)\,d\sigma\,\mathbf{c}_V$$

for all $\tau \in \mathcal{T}$, with $\mathbf{F}(\sigma) = \left[\,\mathbf{F}_1^T(\sigma) \quad \cdots \quad \mathbf{F}_m^T(\sigma)\,\right]^T$. The first derivative is simply given by

$$\frac{\partial}{\partial \tau}\mathbf{f}(t_0, \tau) = \mathbf{T}_M(\tau)\,\mathbf{F}(\tau)\,\mathbf{c}_V$$

where for the limit points $\tau = t_0$ and $\tau = t_f$, with a slight abuse of notation, the derivative is considered to be, respectively, the right and left derivatives of $\mathbf{f}$. The second derivative is given by

$$\frac{\partial^2}{\partial \tau^2}\mathbf{f}\,(t_0,\tau) = \left(\dot{\mathbf{T}}_{M}\,(\tau)\,\mathbf{F}(\tau) + \mathbf{T}_{M}\,(\tau)\,\dot{\mathbf{F}}(\tau)\right)\mathbf{c}_V$$

where the first derivative of the components of $\mathbf{F}(\tau)$ is

$$\frac{d\,\mathbf{F}_i(\tau)}{d\tau} = \dot{\mathbf{F}}_i(\tau) = \begin{bmatrix} \mathbf{0}_{2\times 2} & \mathbf{S}\,\dot{\mathbf{y}}_{p_i}\,(\tau) \\ \mathbf{0}_{2\times 2} & \mathbf{S}\,\dot{\mathbf{y}}_{d_i}\,(\tau) \end{bmatrix}.$$

Suppose now that the observability Gramian $\boldsymbol{\mathcal{W}}\,(t_0,t_f)$ is not invertible. Then, there exists a unit vector $\mathbf{c}$ such that

$$\mathbf{c}^T\,\boldsymbol{\mathcal{W}}\,(t_0,t)\;\mathbf{c} = 0 \tag{7}$$

for all $t \in \mathcal{T}$, which in turn implies that $\mathbf{f}\,(t_0,t) = \mathbf{0}$ and $\frac{\partial}{\partial t}\mathbf{f}\,(t_0,t) = \mathbf{0}$ for all $t \in \mathcal{T}$. In particular, for $t = t_0$, this immediately implies that $\mathbf{c}_i = \mathbf{0}\ \forall_{i=1,\ldots,m}$. Then, under conditions 1 or 2 of the theorem, the only solution of $\frac{\partial}{\partial t}\mathbf{f}\,(t_0,t) = \mathbf{0}$ for all $t \in \mathcal{T}$ is $\mathbf{c}_v = \mathbf{0}$ and $c_b = 0$, as the result of Assumption 1. Moreover, under condition 3, it can be seen that $\frac{\partial}{\partial t}\mathbf{f}\,(t_0,t) = \mathbf{0}$ for all $t \in \mathcal{T}$ is equivalent to

$$-\mathbf{c}_v + \mathbf{S}\,\mathbf{y}_{p_1}(t)\,c_b = \mathbf{0}$$

for all $t \in \mathcal{T}$, and taking the time derivative on both sides it becomes

$$\mathbf{S}\,\dot{\mathbf{y}}_{p_1}(t)\,c_b = \mathbf{0}$$

for all $t \in \mathcal{T}$. In particular, for $t = t_1$, the only solution is $c_b = 0$, and thus, the former equation implies that $\mathbf{c}_v = \mathbf{0}$. Either way, this contradicts the existence of a unit vector $\mathbf{c}$ such that (7) holds for all $t \in \mathcal{T}$. As such, the observability Gramian $\boldsymbol{\mathcal{W}}\,(t_0,t_f)$ is invertible on $\mathcal{T}$, and from Lemma 1, the nonlinear system (6), regarded as LTV, is observable on $\mathcal{T}$, thus, concluding the proof of the theorem. ■

With these sufficient conditions for observability, a practical result on the design of an observer for the nominal nonlinear system is presented in the following theorem. An example of this approach can also be found in [27].

Theorem 3: If the conditions of Theorem 2 hold, then

1) the initial state of both the nonlinear system (4), regarded as LTV, and the nominal nonlinear system (3) are the same and uniquely determined;
2) a state observer with uniformly globally asymptotically stable error dynamics for the LTV system is also a state observer for the underlying nonlinear system, with uniformly globally asymptotically stable error dynamics.

Proof: As in the previous theorem, the nonlinear system (6) is considered for simplicity of analysis, noting that the Lyapunov transformation preserves all the properties provided in this proof for the system (4).

Consider the initial condition for the nonlinear system (6), regarded as LTV, given by

$$\bar{\mathbf{z}}(t_0) = \left[\,\bar{\mathbf{v}}^T(t_0) \quad \bar{b}_r(t_0) \quad \bar{\mathbf{z}}_1^T(t_0) \quad \ldots \quad \bar{\mathbf{z}}_m^T(t_0)\,\right]^T$$

where $\bar{\mathbf{z}}_i(t) = \left[\,\bar{\mathbf{z}}_{p_i}^T(t) \quad \bar{\mathbf{z}}_{d_i}^T(t)\,\right]^T$, for landmarks with one associated direction. It is also noted that $\mathbf{y}(t) = \boldsymbol{\mathcal{C}}(t)\,\mathbf{z}(t)$ implies that $\bar{\mathbf{z}}_{p_i} = \mathbf{R}_g(t)\,\mathbf{y}_{p_i}(t)$ and $\bar{\mathbf{z}}_{d_i} = \mathbf{R}_g(t)\,\mathbf{y}_{d_i}(t)$ for all $t \in \mathcal{T}$. Then, it can be seen that the output of the nonlinear system (6), regarded as LTV, as a function of the initial conditions is defined by $\mathbf{y}(t) = \boldsymbol{\mathcal{C}}(t)\,\boldsymbol{\phi}\,(t,t_0)\;\bar{\mathbf{z}}(t_0)$, yielding

$$\begin{aligned}\mathbf{y}_{p_i}(t) &= \mathbf{R}_g^T(t)\,\bar{\mathbf{z}}_{p_i}(t_0) \\ &\quad + \mathbf{R}_g^T(t)\int_{t_0}^{t}\mathbf{R}_g(\sigma)\left[\mathbf{S}\,\mathbf{y}_{p_i}(\sigma)\,\bar{b}_r(t_0) - \bar{\mathbf{v}}(t_0)\right]d\sigma \\ &= \mathbf{R}_g^T(t)\,\mathbf{R}_g(t_0)\,\mathbf{y}_{p_i}(t_0) \\ &\quad + \mathbf{R}_g^T(t)\int_{t_0}^{t}\mathbf{R}_g(\sigma)\left[\mathbf{S}\,\mathbf{y}_{p_i}(\sigma)\,\bar{b}_r(t_0) - \bar{\mathbf{v}}(t_0)\right]d\sigma \end{aligned} \tag{8}$$

for all $t \in \mathcal{T}$ and $i \in \mathcal{I}_o$, noting that a similar expression can be derived for the output of each landmark direction. Multiplying both sides by $\mathbf{R}_g(t)$ and rearranging the terms, (8) becomes

$$\begin{aligned}&\mathbf{R}_g(t)\,\mathbf{y}_{p_i}(t) - \mathbf{R}_g(t_0)\,\mathbf{y}_{p_i}(t_0) \\ &\quad = \int_{t_0}^{t}\mathbf{R}_g(\sigma)\left(-\bar{\mathbf{v}}(t_0) + \mathbf{S}\,\mathbf{y}_{p_i}(\sigma)\bar{b}_r(t_0)\right)d\sigma\end{aligned}$$

and differentiation of both sides yields

$$\begin{aligned}&\dot{\mathbf{R}}_g(t)\,\mathbf{y}_{p_i}(t) + \mathbf{R}_g(t)\,\dot{\mathbf{y}}_{p_i}(t) \\ &\quad = \mathbf{R}_g(t)\left(-\bar{\mathbf{v}}(t_0) + \mathbf{S}\,\mathbf{y}_{p_i}(t)\,\bar{b}_r(t_0)\right)\end{aligned}$$

which can be further simplified recalling that $\dot{\mathbf{R}}_g(t) = r_g(t)\;\mathbf{R}_g(t)\,\mathbf{S}$,

$$\dot{\mathbf{y}}_{p_i}(t) = -[r_g(t) - \bar{b}_r(t_0)]\,\mathbf{S}\,\mathbf{y}_{p_i}(t) - \bar{\mathbf{v}}(t_0)$$

and differentiating both sides once more results in the second-order derivative

$$\ddot{\mathbf{y}}_{p_i}(t) = -[r_g(t) - \bar{b}_r(t_0)]\,\mathbf{S}\,\dot{\mathbf{y}}_{p_i}(t) - \dot{r}_g(t)\,\mathbf{S}\,\mathbf{y}_{p_i}(t).$$

Using the same procedure for the landmark directions, it can be seen that $\dot{\mathbf{y}}_{d_i}(t) = -[r_g(t) - \bar{b}_r(t_0)]\,\mathbf{S}\,\mathbf{y}_{d_i}(t)$ and

$$\ddot{\mathbf{y}}_{d_i}(t) = -[r_g(t) - \bar{b}_r(t_0)]\,\mathbf{S}\,\dot{\mathbf{y}}_{d_i}(t) - \dot{r}_g(t)\,\mathbf{S}\,\mathbf{y}_{d_i}(t).$$

Consider now the initial condition for the nominal nonlinear system (3) given by

$$\mathbf{x}(t_0) = \left[\,\mathbf{v}(t_0) \quad b_r(t_0) \quad \mathbf{x}_1^T(t_0) \quad \ldots \quad \mathbf{x}_m^T(t_0)\,\right]$$

where $\mathbf{x}_i(t) = \left[\,\mathbf{p}_i^T(t) \quad \mathbf{d}_i^T(t)\,\right]^T$. It can be seen that the output of the nonlinear system as a function of the initial condition is given by $\mathbf{y}(t) = \mathbf{C}\,\mathbf{x}(t)$, yielding

$$\mathbf{y}_{p_i}(t) = \mathbf{p}_i(t_0) - \int_{t_0}^{t}\left([r_g(\sigma) - b_r(\sigma)]\mathbf{S}\,\mathbf{p}_i(\sigma) + \mathbf{v}(\sigma)\right)d\sigma$$

and

$$\mathbf{y}_{d_i}(t) = \mathbf{d}_i(t_0) - \int_{t_0}^{t}[r_g(\sigma) - b_r(\sigma)]\mathbf{S}\,\mathbf{d}_i(\sigma)d\sigma$$

for all $t \in \mathcal{T}$ and $i \in \mathcal{I}_o$. Noting that $\mathbf{v}(t)$ and $b_r(t)$ are constant, the first-order derivatives of the aforementioned expressions are given by

$$\dot{\mathbf{y}}_{p_i}(t) = -[r_g(t) - b_r(t_0)]\mathbf{S}\,\mathbf{p}_i(t) - \mathbf{v}(t_0)$$

and

$$\dot{\mathbf{y}}_{d_i}(t) = -[r_g(t) - b_r(t_0)]\mathbf{S}\,\mathbf{d}_i(t)$$

for all $t \in \mathcal{T}$ and $i \in \mathcal{I}_O$. It is relevant to note that the aforementioned expressions imply $\dot{\mathbf{y}}_{p_i}(t) = \dot{\mathbf{p}}_i(t)$ and $\dot{\mathbf{y}}_{d_i}(t) = \dot{\mathbf{d}}_i(t)$, also for all $t \in \mathcal{T}$ and $i \in \mathcal{I}_O$. Furthermore, the second-order derivatives are given by

$$\ddot{\mathbf{y}}_{p_i}(t) = -[r_g(t) - b_r(t_0)]\mathbf{S}\,\dot{\mathbf{p}}_i(t) - \dot{r}_g(t)\mathbf{S}\,\mathbf{p}_i(t)$$

and

$$\ddot{\mathbf{y}}_{d_i}(t) = -[r_g(t) - b_r(t_0)]\mathbf{S}\,\dot{\mathbf{d}}_i(t) - \dot{r}_g(t)\mathbf{S}\,\mathbf{d}_i(t)$$

for all $t \in \mathcal{T}$ and $i \in \mathcal{I}_O$.

In particular, comparing the first-order derivatives of the output of the LTV system and the output the nominal nonlinear system for $t = t_1$, noting that $\mathbf{y}_{p_i}(t_1) = \mathbf{p}_i(t_1)$ and $\mathbf{y}_{d_i}(t_1) = \mathbf{d}_i(t_1)$ for all $i \in \mathcal{I}_O$, it can be seen that

$$0 = [b_r(t_0) - \bar{b}_r(t_0)]\mathbf{S}\,\mathbf{y}_{p_i}(t_1) - [\mathbf{v}(t_0) - \bar{\mathbf{v}}(t_0)]$$

and

$$0 = [b_r(t_0) - \bar{b}_r(t_0)]\mathbf{S}\,\mathbf{y}_{d_i}(t_1)$$

for all $i \in \mathcal{I}_O$. The first condition of Theorem 2 yields

$$\begin{cases} 0 = [\bar{b}_r(t_0) - b_r(t_0)]\mathbf{S}\,\mathbf{y}_{p_1}(t_1) + [\mathbf{v}(t_0) - \bar{\mathbf{v}}(t_0)] \\ 0 = [\bar{b}_r(t_0) - b_r(t_0)]\mathbf{S}\,\mathbf{y}_{p_2}(t_1) + [\mathbf{v}(t_0) - \bar{\mathbf{v}}(t_0)] \end{cases}$$

whereas the second condition yields

$$\begin{cases} 0 = [\bar{b}_r(t_0) - b_r(t_0)]\mathbf{S}\,\mathbf{y}_{p_1}(t_1) + [\mathbf{v}(t_0) - \bar{\mathbf{v}}(t_0)] \\ 0 = [\bar{b}_r(t_0) - b_r(t_0)]\mathbf{S}\,\mathbf{y}_{d_1}(t_1). \end{cases}$$

Thus, the only solution for the set of equations derived for each condition is $\bar{b}_r(t_0) = b_r(t_0)$ and $\bar{\mathbf{v}}(t_0) = \mathbf{v}(t_0)$. For the third condition, it can be seen that the comparison of the first- and second-order derivatives for $t = t_1$ yields

$$\begin{cases} 0 = [\bar{b}_r(t_0) - b_r(t_0)]\mathbf{S}\,\mathbf{y}_{p_1}(t_1) + [\mathbf{v}(t_0) - \bar{\mathbf{v}}(t_0)] \\ 0 = [\bar{b}_r(t_0) - b_r(t_0)]\mathbf{S}\,\dot{\mathbf{y}}_{p_1}(t_1) \end{cases}$$

which, for $\dot{\mathbf{y}}_{p_1}(t_1) \neq 0$, implies that the only solution for the aforementioned system of equations is also $\bar{b}_r(t_0) = b_r(t_0)$ and $\bar{\mathbf{v}}(t_0) = \mathbf{v}(t_0)$.

It is noted that the state of the nonlinear system (4) is related through the Lyapunov transformation $\mathbf{T}(t)$ with the state of the nonlinear system (6). Therefore, under the conditions of Theorem 2, the state of the nonlinear system (4), regarded as LTV, and the state of the nominal nonlinear system (3) are the same and uniquely defined, provided the knowledge about the evolution of $\mathbf{y}(t)$ and $r_g(t)$ for all $t \geq t_0$.

The second part of the theorem follows from this conclusion. The estimation error of an observer designed for the LTV system with globally asymptotically stable error dynamics converges to zero, which means that its estimates asymptotically approach the true state. However, as the true state of the LTV system matches that of the nominal nonlinear system, that means that the observer for the LTV system is also an observer for the nominal nonlinear system, with GAS error dynamics. ■

The next result shows that there is no conservativeness whatsoever in the conditions of Theorem 2, as they are necessary and sufficient for the observability of the nominal nonlinear system. While the first two conditions of Theorem 2 are two well-known examples of how to observe the pose of a vehicle in 2-D, the importance of the third condition arises when proving necessity in the following result. Indeed, when only one landmark is visible and the vehicle is moving exactly in a circle around that landmark with the same relative bearing, the system becomes unobservable. Conversely, if either the relative bearing or the distance to that landmark varies through time, the pose of the vehicle is observable.

Theorem 4: The nonlinear system (3) is observable on $\mathcal{T} = [t_0, t_f]$, if and only if the conditions of Theorem 2 hold.

Proof: The sufficiency part is readily provided by Theorems 2 and 3, assuming that the output signal $\mathbf{y}(t)$ is known for all $t \in \mathcal{T}$. The proof of necessity is achieved by transposition, i.e., if none of the conditions of the theorem are met, then the nonlinear system (3) must be unobservable, in the sense that, there exists a system output for which the initial condition is not unique. The proof will proceed toward this goal, noting that this is equivalent to find, at least, two different initial conditions for which the generated output is exactly the same.

Recalling the landmark nonlinear dynamic equations defined in (1), the output solution for the nonlinear system (3), as a function of the initial conditions, can be defined as

$$\begin{aligned} \mathbf{y}(t) = \mathbf{p}_1(t) &= \mathbf{p}_1(t_0) + \int_{t_0}^{t} \dot{\mathbf{p}}_1(\sigma)d\sigma \\ &= \mathbf{p}_1(t_0) - \int_{t_0}^{t} \left(\mathbf{v}(\sigma) + [r_g(\sigma) - b_r(\sigma)]\,\mathbf{S}\,\mathbf{p}_1(\sigma)\right) d\sigma \end{aligned}$$

for all $t \in \mathcal{T}$, when there is only one visible position landmark. The negation of the conditions of the theorem means that either no landmark is visible or there is only one constant visible position landmark, $\mathbf{y}_{p_1}(t) = \mathbf{y}_{p_1}(t_0)$ for all $t \in \mathcal{T}$. As the case where no landmark is visible clearly renders the system unobservable, the proof proceeds with the analysis of the case where there is only one visible position landmark that remains constant for all $t \in \mathcal{T}$. Under this condition, the dynamic constraint $\mathbf{y}_i(t) = \mathbf{x}_i(t)$ for all $i \in \mathcal{I}_O$ and $t \in \mathcal{T}$, implies that $\mathbf{y}_1(t) = \mathbf{y}_{p_1}(t) = \mathbf{p}_1(t) = \mathbf{p}_1(t_0)$ for all $t \in \mathcal{T}$, yielding $\dot{\mathbf{p}}_1(t) = \mathbf{0}$ and

$$\mathbf{v}(t) = -\left[r_g(t) - b_r(t)\right]\,\mathbf{S}\,\mathbf{p}_1(t_0) \tag{9}$$

for all $t \in \mathcal{T}$. As the vehicle dynamics further impose $\dot{\mathbf{v}}(t) = 0$ and $\dot{b}_r(t) = 0$ for all $t \in \mathcal{T}$, it can also be seen that $r_g(t) = r_g(t_0)$ for all $t \in \mathcal{T}$, yielding the system output solution

$$\begin{aligned} \mathbf{y}(t) &= \mathbf{p}_1(t_0) - \int_{t_0}^{t} \left(\mathbf{v}(t_0) + [r_g(t_0) - b_r(t_0)]\,\mathbf{S}\,\mathbf{p}_1(t_0)\right) d\sigma \\ &= \mathbf{p}_1(t_0) - (t - t_0)\left(\mathbf{v}(t_0) + [r_g(t_0) - b_r(t_0)]\,\mathbf{S}\,\mathbf{p}_1(t_0)\right) \end{aligned}$$

for all $t \in \mathcal{T}$.

Consider two different initial conditions for system (5) given by $\mathbf{x}_a(t_0) = [\,\mathbf{v}_a^T(t_0) \quad b_r(t_0) \quad \mathbf{p}_1^T(t_0)\,]^T$ and $\mathbf{x}_b(t_0) = [\mathbf{v}_b^T(t_0) \quad \alpha\, b_r(t_0) \quad \mathbf{p}_1^T(t_0)]^T$, where $\alpha \neq 0 \in \mathbb{R}$ and there is only one position landmark, such that the initial velocities are defined as $\mathbf{v}_a(t_0) = -\left[r_g(t_0) - b_r(t_0)\right]\,\mathbf{S}\,\mathbf{p}_1(t_0)$ and $\mathbf{v}_b(t_0) =$

$-[r_g(t_0)-\alpha\, b_r(t_0)]\,\mathbf{S}\,\mathbf{p}_1(t_0)$, Considering the previously computed output solution expression, it is a matter of algebraic manipulation to show that the output solution of (3) for the initial condition $\mathbf{x}_a(t_0)$ is given by

$$\begin{aligned}\mathbf{y}_a(t) &= \mathbf{p}_1(t_0)-(t-t_0)\,(\mathbf{v}_a(t_0)+[r_g(t_0)-b_r(t_0)]\,\mathbf{S}\,\mathbf{p}_1(t_0))\\ &= \mathbf{p}_1(t_0)-(t-t_0)\,(\mathbf{v}_a(t_0)-\mathbf{v}_a(t_0))\end{aligned}$$

for all $t\in\mathcal{T}$, whereas the output for the second initial condition, $\mathbf{x}_b(t_0)$, is given by

$$\begin{aligned}\mathbf{y}_b(t) &= \mathbf{p}_1(t_0)-(t-t_0)\,(\mathbf{v}_b(t_0)+[r_g(t_0)-\alpha\, b_r(t_0)]\,\mathbf{S}\,\mathbf{p}_1(t_0))\\ &= \mathbf{p}_1(t_0)-(t-t_0)\,(\mathbf{v}_b(t_0)-\mathbf{v}_b(t_0))\end{aligned}$$

for all $t\in\mathcal{T}$. From the aforementioned expressions, it can be seen that $\mathbf{y}_a(t)=\mathbf{y}_b(t)=\mathbf{p}_1(t_0)$ for all $t\in\mathcal{T}$, meaning that there are at least two different initial conditions for which the output of the system is the same. This implies that the system is unobservable on $\mathcal{T}$. Therefore, if none of the conditions of the theorem are satisfied, then system (3) is unobservable, which proves the necessity of those conditions, thus concluding the proof. ∎

With the previous results, the design of a filter for the system (4) regarded as LTV, with globally asymptotically stable error dynamics follows naturally with a LTV Kalman filter, provided that the pair $(\mathbf{A}(t),\mathbf{C}(t))$ is UCO. The following proposition is used throughout the proof of Theorem 6.

Proposition 5 ([20, Proposition 4.2]): Let $\mathbf{g}(t_1,t_2):\mathcal{T}\times\mathcal{T}\subset\mathbb{R}^2\rightarrow\mathbb{R}^n$ be a continuous and i times continuously differentiable function on $\mathcal{T}:=[t_0,t_f]$, $T:=t_f-t_0>0$, and such that

$$\mathbf{g}\,(t_0,t_0)=\left.\frac{\partial\,\mathbf{g}\,(t_0,\tau)}{\partial\tau}\right|_{\tau=t_0}=\cdots=\left.\frac{\partial^{i-1}\,\mathbf{g}\,(t_0,\tau)}{\partial\tau^{i-1}}\right|_{\tau=t_0}=\mathbf{0}.$$

Further assume that $\|\frac{\partial^{i+1}\,\mathbf{g}(t_0,\tau)}{\partial\tau^{i+1}}|_{\tau=t}\|\leq C$ for all $t\in\mathcal{T}$. If there exists a positive constant $\alpha>0$ and a time instant $t\in\mathcal{T}$ such that $\|\frac{\partial^{i}\,\mathbf{g}(t_0,\tau)}{\partial\tau^{i}}|_{\tau=t}\|\geq\alpha$, then there exists $0<\delta\leq T$ and a positive constant $\beta>0$ such that $\|\mathbf{g}(t_0,t_0+\delta)\|\geq\beta$.

A generalization of Assumption 1 is also introduced, which considers upper and lower bounds for the norms of each landmark and for the differences between them. This is also a realistic assumption, as in a Laser scanner there are upper and lower bounds for both range and bearing measurements. The necessity of this generalization emerges from the need to establish uniform bounds when proving UCO.

Assumption 2: For any detected landmark $i\in\mathcal{I}_O$, there exist $\bar{\alpha}_p>0$, $\alpha_{p_i}>0$, $\bar{\alpha}_d>0$, and $\alpha_{d_i}>0$ such that $\bar{\alpha}_p\geq\|\mathbf{y}_{p_i}(t)\|\geq\alpha_{p_i}$ and $\bar{\alpha}_d\geq\|\mathbf{y}_{d_i}(t)\|\geq\alpha_{d_i}$ for all $t\geq t_0$. Furthermore, for any two detected position landmarks $i,j\in\mathcal{I}_O$, with $i\neq j$, there exist $\alpha_{p_{ij}}>0$ such that $\left\|\mathbf{y}_{p_i}(t)-\mathbf{y}_{p_j}(t)\right\|\geq\alpha_{p_{ij}}$ for all $t\geq t_0$.

As stronger forms of observability are needed when dealing with LTV systems, the following result establishes the conditions under which the pair $(\mathbf{A}(t),\mathbf{C}(t))$ is UCB.

Theorem 6: Suppose that Assumption 2 holds. The pair $(\mathbf{A}(t),\mathbf{C}(t))$ is UCB if and only if there exist $\alpha_{\dot{p}}>0$ and $\delta>0$ such that, for all $t\geq t_0$, it is possible to choose $t_1\in\mathcal{T}_\delta$, with $\mathcal{T}_\delta=[t,t+\delta]$, for which there exist, at least, either

1) two visible position landmarks, $\mathbf{y}_{p_1}(t_1)$ and $\mathbf{y}_{p_2}(t_1)$ or
2) one visible position landmark $\mathbf{y}_{p_1}(t_1)$ with, at least, one associated direction $\mathbf{y}_{d_1}(t_1)$ or
3) one visible position landmark $\mathbf{y}_{p_1}(t_1)$ for which the condition $\|\dot{\mathbf{y}}_{p_1}(t_1)\|\geq\alpha_{\dot{p}}$ is satisfied.

Proof: The proof, provided in the Appendix, follows similar steps to the proofs of Theorems 2 and 4, but considering uniform bounds for all $t\geq t_0$ and intervals $[t,t+\delta]$. ∎

The third condition of Theorem 6, which is necessary for the observability of the system when only one landmark is available, may be interpreted as a persistent excitation condition.

The uniform global asymptotic stability of the error dynamics of a continuous-time observer, which can be denoted as

$$\dot{\tilde{\mathbf{x}}}(t)=\tilde{\mathbf{A}}(t)\,\tilde{\mathbf{x}}(t)$$

is achieved by using the Lyapunov function $\mathbf{V}(t,\tilde{\mathbf{x}}(t))=\tilde{\mathbf{x}}^T(t)\,\mathbf{P}^{-1}(t)\,\tilde{\mathbf{x}}(t)$, and under the conditions of Theorem 6, show that $\mathbf{P}^{-1}(t)$ is positive definite and all the conditions of [29, Theorem 8.5] are satisfied globally. This is a standard procedure for LTV systems, and thus, it is omitted, noting that further details can be found in [29, Example 8.11], [30]–[32], and references therein.

IV. Simultaneous Localization and Mapping Filter Design

The design of the sensor-based SLAM filter is presented in this section. As detailed in the previous section, the system (3), regarded as LTV, is UCB under the conditions of Theorem 6. This is an important result that leads naturally to the design of a Kalman filter with globally asymptotically stable error dynamics, noting that other filtering alternatives could be devised, e.g., an $\mathcal{H}_\infty$ filter.

The majority of sensors available today and the processing units used in robotic vehicles are usually sample-based or even intrinsically digital. To profit from those sensors, and the low cost and light weighted embedded computers to be installed on board small platforms, a discrete-time version of the SLAM algorithm is required. Without loss of generality, let T_s denote the sampling period of the synchronized IMU and laser scanner, noting that a multirate implementation of the proposed filter can be devised. Considering that $\mathbf{x}_k:=\mathbf{x}(t_k)$, $\mathbf{A}_k:=\mathbf{A}(t_k)$, and $\mathbf{C}_k:=\mathbf{C}(t_k)$, with $t_k=t_0+k\,T_s$, $k\in\mathbb{N}_0$, and t_0 as the initial time, the forward Euler discretization of the system dynamics (3) yields

$$\begin{cases}\mathbf{x}_{k+1}=\mathbf{F}_k\,\mathbf{x}_k+\boldsymbol{\xi}_k\\ \mathbf{y}_{k+1}=\mathbf{H}_{k+1}\,\mathbf{x}_{k+1}+\boldsymbol{\theta}_{k+1}\end{cases}\tag{10}$$

where $\mathbf{F}_k:=\mathbf{I}_{n_x}+T_s\,\mathbf{A}_k$ and $\mathbf{H}_k:=\mathbf{C}_k$. The system (10) includes system disturbance and measurement noise, where the vectors $\boldsymbol{\xi}_k\in\mathbb{R}^{n_x}$ and $\boldsymbol{\theta}_k\in\mathbb{R}^{n_y}$ are zero-mean discrete white Gaussian noise, with $\langle\boldsymbol{\xi}_k\,\boldsymbol{\xi}_l^T\rangle=\boldsymbol{\Xi}_k\,\delta_{k-l}$ and $\langle\boldsymbol{\theta}_k\,\boldsymbol{\theta}_l^T\rangle=\boldsymbol{\Theta}_k\,\delta_{k-l}$, respectively, where δ_k denotes the Dirac delta function and the expectation operator is denoted by $\langle.\rangle$. It is noted that the dimensions of the discrete system (10) may change dynamically

with the number of visible landmarks obtained with each new laser measurement.

A. Prediction Step

The resulting discrete-time Kalman filter equations for the aforementioned system are standard [31], [33], [34]. Nonetheless, the system (10) does not account for the nonvisible landmarks $\mathbf{x}_{U_k}$, which have to be propagated in open loop using the nonlinear equations defined in (2). Using the full system state vector $\mathbf{x}_{F_k} := \begin{bmatrix} \mathbf{x}_k^T & \mathbf{x}_{U_k}^T \end{bmatrix}^T$, the prediction equations are

$$\begin{cases} \hat{\mathbf{x}}_{F_{k+1|k}} = \mathbf{F}_{F_{k|k}}\, \hat{\mathbf{x}}_{F_{k|k}} \\ \boldsymbol{\Sigma}_{F_{k+1|k}} = \hat{\mathbf{F}}_{F_{k|k}}\, \boldsymbol{\Sigma}_{F_{k|k}}\, \hat{\mathbf{F}}_{F_{k|k}}^T + \boldsymbol{\Xi}_{F_k} \end{cases}$$

where $\hat{\mathbf{x}}_{F_{k|k}}$ denotes the estimated state vector, the disturbance covariance matrix is defined as $\boldsymbol{\Xi}_{F_k} = \text{diag}\left(\boldsymbol{\Xi}_k, \boldsymbol{\Xi}_{U_k}\right)$, whereas the full state covariance matrix $\boldsymbol{\Sigma}_{F_{k|k}}$ can be decomposed in observable, unobservable, and crossed terms, respectively, $\boldsymbol{\Sigma}_{k|k}$, $\boldsymbol{\Sigma}_{U_{k|k}}$, and $\boldsymbol{\Sigma}_{UO_{k|k}}$. The full transition matrix $\mathbf{F}_{F_{k|k}}$ is defined as

$$\mathbf{F}_{F_{k|k}} = \begin{bmatrix} \mathbf{F}_k & \mathbf{0}_{n_x \times n_U} \\ \mathbf{F}_{UO_{k|k}} & \mathbf{F}_{U_{k|k}} \end{bmatrix}$$

where the remaining undefined terms can be inferred from the nominal system dynamics (2), and

$$\hat{\mathbf{F}}_{F_{k|k}} = \frac{\partial\, \mathbf{F}_{F_{k|k}}\, \hat{\mathbf{x}}_{F_{k|k}}}{\partial \hat{\mathbf{x}}_{F_{k|k}}}.$$

B. Update Step

Whenever a new laser profile measurement is obtained, the raw values are projected into the horizontal frame H using the roll and pitch information provided by an external attitude filter. The horizontal laser profile is fed to a landmark detection algorithm, where the data are processed into clusters and a robust line detection strategy is implemented, which builds on the basic split and merge algorithm, see [35], using a reduced space Hough transform parameter fitting for each line, in a similar way to the algorithm proposed in [36]. Afterwards, a corner identification procedure is used to obtain the desired point landmarks. This detection algorithm can provide point landmarks with up to two associated line segments, which may be included in the filtering process as direction landmarks. This is the converse case of having a line landmark with two end points. The association between measured landmarks and existing state landmarks is implemented resorting to the JCBB algorithm; (see [9] for details). In short, this algorithm searches the tree of possible landmark association pairs such that all the associations are jointly compatible in a probabilistic sense. It is noted that the corner detection algorithm and the landmark association algorithm may be replaced by others available, as they are completely independent of the filtering technique proposed in this paper. The sets of visible and nonvisible landmarks, respectively, $\mathcal{I}_{O_k}$ and $\mathcal{I}_{U_k}$, are redefined at each new laser measurement, based on landmark associations provided by the JCBB algorithm. In addition, this algorithm naturally provides the innovation vector, $\boldsymbol{\nu}_{k+1} = \mathbf{y}_{k+1} - \mathbf{H}_{k+1}\, \hat{\mathbf{x}}_{F_{k+1|k}}$, and its respective covariance matrix, $\boldsymbol{\Sigma}_{\nu_{k+1}} = \mathbf{H}_{k+1}\, \boldsymbol{\Sigma}_{F_{k+1|k}}\, \mathbf{H}_{k+1}^T + \boldsymbol{\Theta}_{k+1}$. Thus, for the update step, it is just a matter of applying the standard discrete time-varying Kalman filter update equations.

C. Basic Loop Closing

The loop-closing problem is not the main focus of this study, but rather a demonstration that the proposed filter provides consistent estimates that will enable any loop-closing technique to perform efficiently in real-world scenarios. Any available strategy can be used, such as the partitioning of the total map into smaller statistically independent maps, accounting for the proper joining and merging between them using a common set of landmarks, in a similar fashion to what is proposed in [16] and [37]. One of the main drawbacks of the sensor-based approach to SLAM is the computational complexity that results from having to update all the landmarks. Indeed, the use of the submap strategy allows to limit the number of landmarks in the current state vector, thus limiting the computational complexity.

A basic algorithm is described later and implemented for completeness of the experimental results presented in Section V. The main difficulty when closing a loop is to obtain a coherent map, as older landmarks will tend to have large uncertainty and wrong associations are very likely to happen during the JCBB procedure of the update step, especially for environments with a dense population of landmarks. The basic idea is then to use only a subset of the state landmarks for the current update step association algorithm, $\mathcal{I}_{\text{cur}}$, where only the landmarks that were most recently visible to the vehicle are used. When revisiting an area, this procedure will generate duplicates of older landmarks, which are defined as the set $\mathcal{I}_{\text{old}}$. Therefore, a rather naive loop-closing algorithm is to search periodically for possible landmark associations between the sets $\mathcal{I}_{\text{cur}}$ and $\mathcal{I}_{\text{old}}$, triggering a loop closure if a minimum number of jointly compatible associations are available. The set of state landmarks is then partitioned into the following three sets: 1) current landmarks $\mathcal{I}_{\text{cur}}$; 2) old landmarks $\mathcal{I}_{\text{old}}$; and 3) the landmarks in between the former two sets, $\mathcal{I}_{\text{gap}}$, which are neither used in the current update step JCBB association algorithm nor in the loop-closing association algorithm.

Consider the noise-free association between landmark $i \in \mathcal{I}_{\text{cur}}$ and landmark $j \in \mathcal{I}_{\text{old}}$, using the output vector $\mathbf{z}_{ij_k} := \hat{\mathbf{x}}_{i_{k|k}} - \hat{\mathbf{x}}_{j_{k|k}} = \mathbf{H}_{ij_k}\, \hat{\mathbf{x}}_{F_{k|k}}$. The respective noise covariance matrix is $\boldsymbol{\Theta}_{ij_k} := \mathbf{0}$ and the measurement vector is defined as $\mathbf{y}_{ij_k} := \mathbf{0}$. Thus, the innovation vector and respective covariance matrix, can be adapted for the loop-closing association of these landmarks, yielding $\boldsymbol{\nu}_{ij_k} = -\mathbf{H}_{ij_k}\, \hat{\mathbf{x}}_{F_{k|k}}$ and $\boldsymbol{\Sigma}_{\nu_{ij_k}} = \mathbf{H}_{ij_k}\, \boldsymbol{\Sigma}_{F_{k|k}}\, \mathbf{H}_{ij_k}$. A loop closure takes place if a significant number of valid loop-closing associations are jointly compatible. This test can be computed using a modified version of the JCBB algorithm adapted to the aforementioned loop-closing innovation expressions. With the joint innovation vector and covariance matrix provided by this algorithm, the standard Kalman filter update equations can be used to constraint the two landmarks to be equal and fully correlated, enabling the removal of one of them from the filter state.

V. Experimental Results

This section describes the experimental setup and presents the results for the proposed sensor-based SLAM algorithm, using position-only landmarks for the simplicity of presentation. These results intend to demonstrate the convergence, performance, and consistency properties of the sensor-based SLAM filter. An instrumented quadrotor was driven along a path of about 60 m in an indoor environment with a loop, as shown in Fig. 6, at an average speed of 0.4 m/s. The trajectory described by the vehicle starts near the middle and circulates counterclockwise until some of the first landmarks detected are once again visible, at the lower right corner. This custom built quadrotor UAV, property of the Institute for Systems and Robotics, is equipped with a MEMSENS nanoIMU, a Maxbotix XL sonar for altitude measurements, and a Hokuyo UTM-30LX laser scanning device that provides horizontal profiles of the surroundings.

The covariance matrix for the zero-mean white Gaussian disturbance that affects the vehicle-related state variables is defined as $\mathbf{\Xi}_{v} = T_s \text{ diag}\left(\sigma_v^2\,\mathbf{I}_2, \sigma_{b_r}^2\right)$, with $\sigma_v = 0.1$ m/s, $\sigma_{b_r} = 5.7 \times 10^{-5}$ deg/s, and the covariance matrix of the disturbance that affect each landmark position is given by $\mathbf{\Xi}_{\mathbf{p}_i} = T_s\,\sigma_p^2\,\mathbf{I}_2$, $\sigma_p = 0.05$ m, for all $i \in \mathcal{I}_k$. The landmark position measurement noise covariance matrix is given as a function of ρ_{i_m} and α_{i_m}, which are the correspondent range and bearing coordinates of the detected landmark $\mathbf{p}_{i_m}$, as well as function of the angular and range standard deviation values, $\sigma_\alpha = 3.75$ deg, $\sigma_{\rho_1} = 0.15$ m, and $\sigma_{\rho_2} = 0.25$ m. Thus, the landmark position measurement noise covariance matrix is defined as

$$\mathbf{\Theta}_{\mathbf{p}_{i_m}} = \sigma_{\rho_{i_m}}^2\,\mathbf{M}_{\alpha_{i_m}} + \sigma_\alpha^2\,\frac{d\,\mathbf{M}_{\alpha_{i_m}}}{d\alpha}$$

assuming a small angle approximation such that $\mathbf{M}_\alpha = \mathbf{R}_\alpha\,\text{diag}(1,0)\,\mathbf{R}_\alpha^T$, where $\mathbf{R}_\alpha$ is the 2-D rotation matrix obtained from an angle α. The range measurement noise of the laser sensor depends on the distance to the detected target, yielding $\sigma_{\rho_{i_m}} = \sigma_{\rho_1}$ if $\rho_{i_m} \leq 10$ m and $\sigma_{\rho_{i_m}} = \sigma_{\rho_2}$ if $\rho_{i_m} > 10$ m. It is noted that the above implicit linearization, always performed at the measured values, is just a way to properly approximate the sensor noise and does not affect any of the SLAM filter properties.

When analyzing the convergence properties of any navigation filter, one of the main goals is to observe a decreasing uncertainty in all variables. This can be seen in Fig. 2(a), where the uncertainty of all the vehicle-related variables decreases over time. Furthermore, it can be seen that the uncertainty of each landmark decreases whenever it is visible and increases otherwise, as shown in Fig. 2(b). The proposed SLAM filter also provides estimates of the linear motion quantities of the vehicle, shown in Fig. 3, along with the remaining vehicle-related variables, without resorting to standard odometry sensors, which are not available for aerial vehicles. These results also show that the constant velocity assumption can be relaxed with the appropriate choice of the filter parameters, in particular σ_v. Although there is an underlying tradeoff, as the velocity uncertainty will also propagate to the uncertainty of the nonvisible landmarks, the presented results indicate that the filter was able to cope with

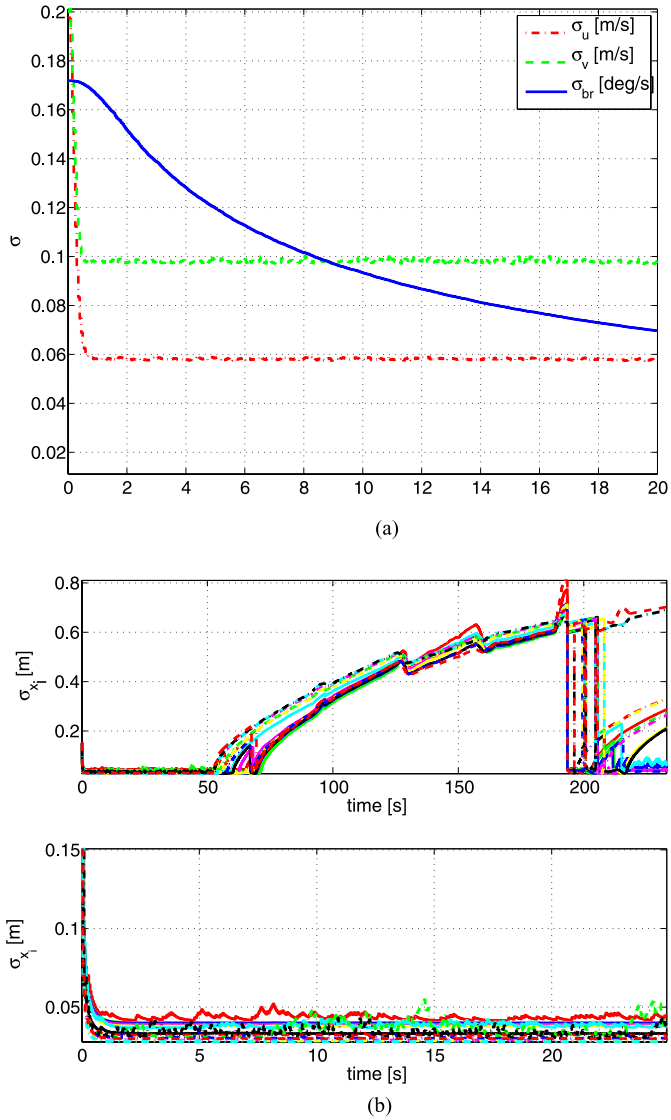

Fig. 2. Convergence of the uncertainty of the sensor-based SLAM filter variables. (a) Standard deviation of the vehicle-related variables: linear velocity and gyro rate bias. (b) Standard Deviation of the first 15 landmark positions to be visible in the sensor-based frame (x-coordinate only). (Top) Complete time evolution. (Bottom) First 25 s.

peaks of 4 m/s^2 of acceleration, without introducing too much conservativeness in the uncertainty of the nonvisible landmarks.

A basic measure of consistency of a SLAM algorithm, when ground truth data are not available, is the maximum normalized innovation squared (NIS) value at each time instant, considering all the landmark associations. As the NIS value for each landmark association is χ^2 distributed with $n_m = \dim(\mathbf{x}_i)$ degrees of freedom, it can be compared, for instance, with the 95% confidence threshold such that

$$\text{NIS}_{i_k} = \boldsymbol{\nu}_{i_k}\,\mathbf{\Sigma}_{\nu_{i_k}}\,\boldsymbol{\nu}_{i_k} \leq \chi^2_{n_m,\,95\%}. \tag{11}$$

This comparison is presented in Fig. 4, along with an average value, where it can be seen that the maximum value seldomly approaches the threshold and it is mostly concentrated below

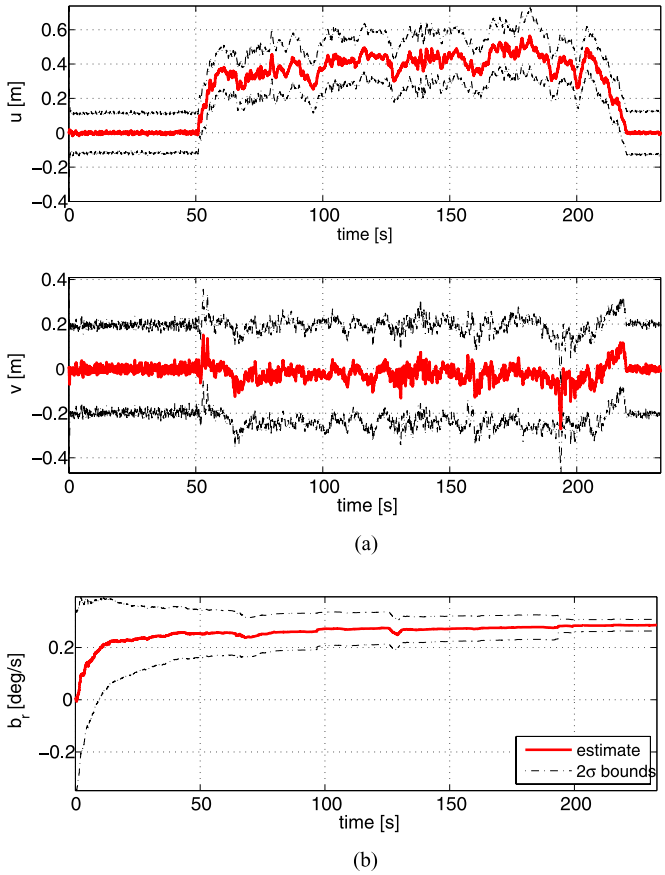

Fig. 3. Time evolution of the vehicle-related state variables (solid red), with $2\,\sigma$ bounds (dash-dotted black). (a) Linear velocity. (b) Rate Gyro bias.

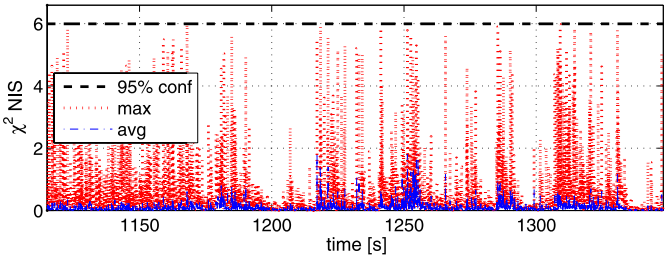

Fig. 4. NIS association: maximum (red), average (blue), and 95% confidence threshold (dashed-dotted black).

$\chi^2_{n_m} = 2$, which might indicate some degree of conservativeness of the filter parameters.

Fig. 5 provides the evolution of the number of landmarks: 1) in the state vector; 2) being visible; and 3) the number of landmark associations being considered for loop closure, including the minimum threshold to enable the loop-closure procedure. From the number of state landmarks, it can be observed that a basic landmark management is done to avoid spurious landmarks due to bad detection. The criteria to delete a landmark is 1) not visible for a long time while it should be in the field of view; 2) intermittently visible in the past, less than an acceptable number of times; and 3) maximum number of landmarks supported is reached, in which case the nonvisible landmark with the highest uncertainty is deleted. This last case is highly undesirable,

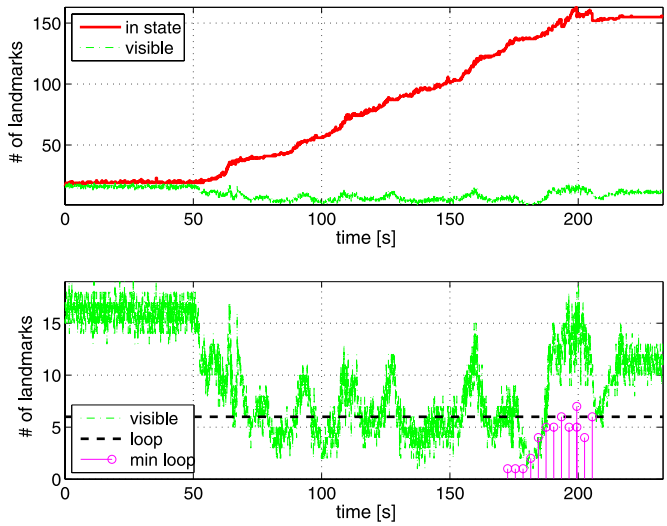

Fig. 5. Time evolution of the number of landmarks. (Top) Number of landmarks in the filter state (solid red) and the number of visible landmarks (dash-dotted green), noting that the latter is always less than the former. (Bottom) Detail on the number of visible landmarks, the number of landmarks used for loop closing (solid magenta), and the minimum loop-closing threshold (dashed black horizontal line).

as it implies the loss of important information, and it does not occur in the experiments provided in this paper. Recalling the conditions of Theorem 2, the number of visible landmarks is always above two, with some exceptions where there was only one visible landmark while the vehicle was moving. Although this is an intrinsic characteristic of the surrounding environment, provided a landmark detection algorithm and respective choice of parameters, it shows that the conditions for observability and convergence of the filter are satisfied in the presented real-world experiments.

The outcome of a SLAM algorithm is twofold 1) self-localization and 2) map construction of the environment. In sensor-based SLAM, the vehicle is deterministically localized at the origin and aligned with the sensor frame. As for the mapping, the proposed SLAM filter provides at each instant a map of the environment in the sensor frame, with consistent uncertainty estimates. The sensor-based map is presented in Fig. 6, featuring the final results of the experimental trial. The landmarks and their respective 95% confidence (or $2\,\sigma$) bounds are shown in three different styles (solid magenta, dashed yellow, and dash-dotted light blue), which denote, respectively, the three sets of landmarks used for the loop-closing step, $\mathcal{I}_{\mathrm{cur}}$, $\mathcal{I}_{\mathrm{gap}}$, and $\mathcal{I}_{\mathrm{old}}$. For completeness, the Earth-fixed reference frame, which was added to the sensor-based SLAM filter as a nonvisible landmark, is shown in the sensor-based map (axes shown in red and green, position and uncertainty in dark blue). This additional nonvisible landmark does not interfere with the observability or convergence analysis, as its state is not used by any other state or measurement equation. The vehicle trajectories (in green), which are computed using an optimization-based algorithm similar to the one proposed in [22], are also shown in the same figure. The main aspects to retain from this intricate figure are the quality of the sensor-based map generated by the

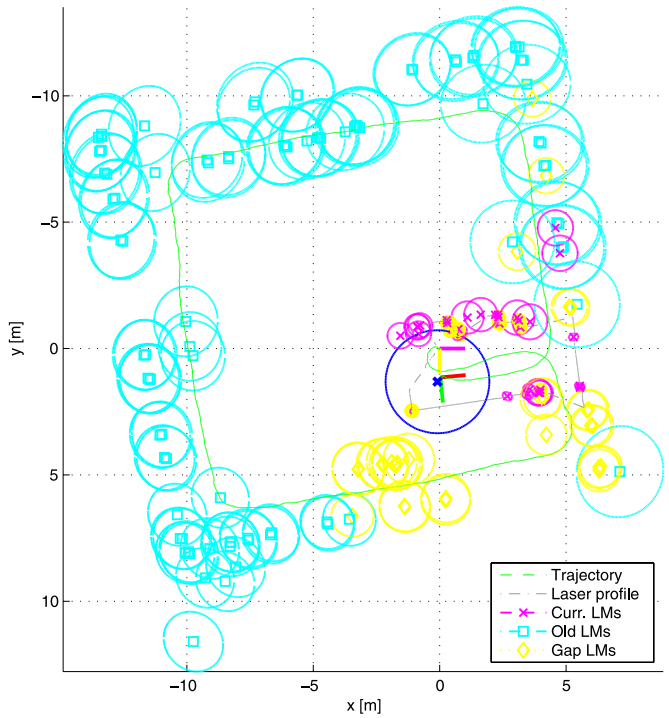

Fig. 6. Map of environment in the sensor frame. This figure shows the current laser profile (in gray), the landmarks in $\mathcal{I}_{\rm cur}$ (in magenta crosses), as well as the landmarks in $\mathcal{I}_{\rm old}$ and $\mathcal{I}_{\rm gap}$ (respectively, in light-blue squares and yellow diamonds) along with their 95% confidence bounds. The Earth-fixed trajectory of the vehicle is also shown for completeness (in dashed green).

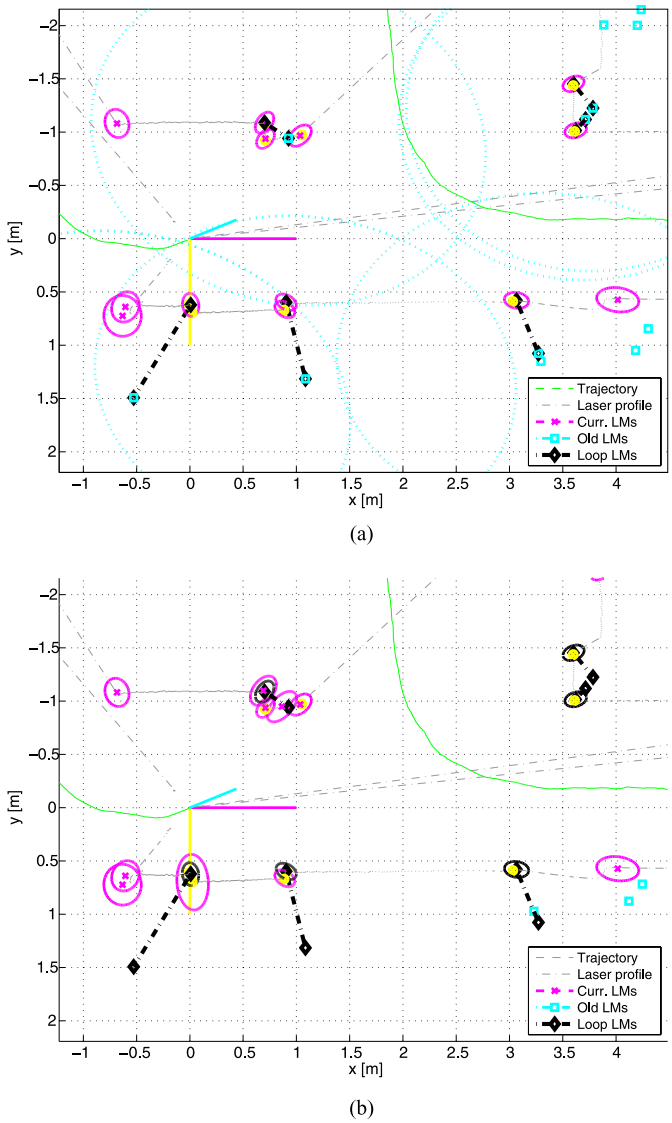

Fig. 7. Detailed view of the map and trajectory in H, showing the 95% confidence bounds of landmarks in $\mathcal{I}_{\rm cur}$ (in magenta), 95% confidence bounds of landmarks in $\mathcal{I}_{\rm old}$ that are being considered for loop closing (in light-blue), and the landmark loop-closing associations and resulting 95% confidence bounds (in black). The sensor-based trajectory of the vehicle is also shown for completeness (in dashed green). (a) Before loop closure. (b) After loop closure.

algorithm, the small uncertainty for the landmarks that were recently visible, and the large uncertainty for the landmarks that are not visible for a long time, as the vehicle progresses along environment.

The practical validation of the consistency of SLAM algorithms occurs in a scenario were the vehicle explores new terrain and at some point returns to a previously visited area, possibly from a different perspective than before. In the experimental results presented in this paper, a loop is closed only three times, the first of which occurs at $t = 193.4$ s, as depicted in Fig. 5. When the vehicle turns at each corner of the building, some older landmarks are observed again, which has a similar effect of a loop closure, but is not considered here as such. To be consistent, the filter uncertainty must allows the association of the currently visible landmarks and the ones observed when the same area was previously visited. The moments just before and right after the loop closure are captured in Fig. 7, where a detailed version of the map of Fig. 6 is presented. The landmark associations between the sets $\mathcal{I}_{\rm cur}$ and $\mathcal{I}_{\rm old}$ are shown in solid black and the fused landmarks positions and uncertainty bounds obtained after the loop closure are also depicted in solid black. It can be seen that the sensor-based map is consistent, allowing for an effective loop closure when revisiting the same area. The successive loop closures that occur in this experiment lead to the consistent correction of the environment map, in particular those landmarks closer to the current position of the vehicle. Although the revisited landmarks suffer a great decrease in uncertainty and their position is corrected, it can also be observed in Fig. 6 that the position of the nearby nonvisible landmarks is also corrected accordingly. This is a consequence of the cross-correlation terms in the state covariance matrix, which enable the propagation of recent innovations to the nonvisible landmarks. It is also noted that for loop-closing purposes, only the information provided by the sensor-based filter is used.

Using an algorithm similar to what is proposed in [22], by resorting to the optimal closed-form solution of the problem of estimating the body to Earth transformation from the landmark position estimates in both frames, the vehicle attitude, position, and the environment map described in the Earth-fixed reference frame can be computed. An example of the map and trajectory described in the Earth-fixed reference frame are presented in Fig. 8.

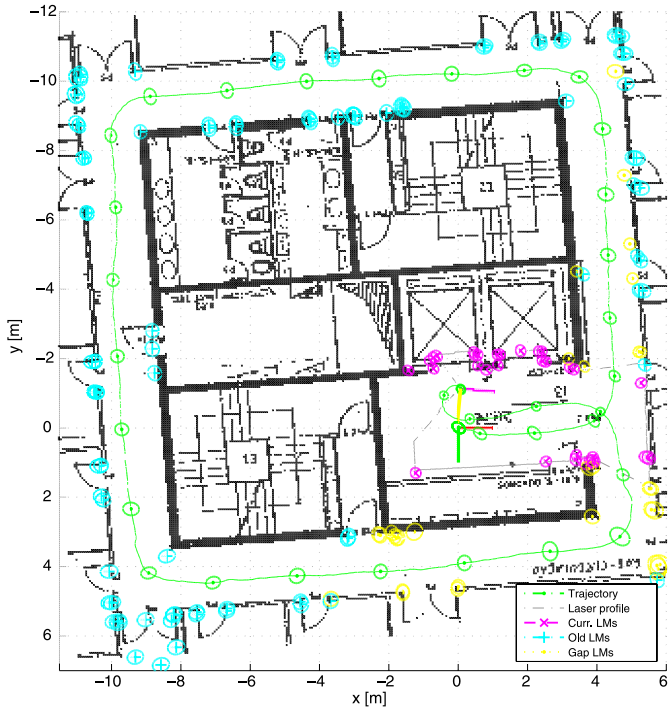

Fig. 8. Map and trajectory in the Earth-fixed reference frame, obtained using an optimization-based trajectory and the map estimation algorithm, with the floor blueprint on the background.

VI. Conclusion and Future Work

This paper presented the design, analysis, and experimental performance evaluation of a novel globally asymptotically stable sensor-based SLAM filter. As opposed to traditional EKF-SLAM algorithms, the proposed method avoids the attitude representation of the vehicle in the filter state, enabling the modification of the nominal nonlinear dynamics into a structure that can be regarded as LTV for analysis and filter design and ultimately, the error dynamics result globally asymptotically stable. The filter does not rely on any odometry sensor, but rather on angular rate measurements, having the byproduct of estimating the linear velocity and the rate gyro bias in the vehicle frame.

The performance and consistency of the proposed SLAM filter are validated in a real-world indoors environment. The sensor-based filter shows the reduction of the uncertainty in every state variable but the nonvisible landmarks and produces a consistent map that is used to close a 60-m long loop. It is also noted that the vehicle attitude, position, and the estimated environment map described in Earth-fixed reference frame can be computed resorting to an optimal closed-form solution of the problem of estimating the body to Earth transformation from the landmark position estimates in both frames.

Future work includes the implementation of a more general loop-closure method such as the division of the total map into submaps, the real-time optimized implementation and testing of the algorithm in UAVs, and the comparison in terms of performance and consistency of the proposed method with the state-of-the-art EKF-SLAM algorithms. Generalizing these results for bearing only or range only measurements as well as the fusion of accelerometer measurements are also great topics for further research.

Appendix
Proof of Theorem 6

The proof of Theorem 6 follows similar steps to the proofs of Theorems 2 and 4, but considering uniform bounds for all $t \geq t_0$ and intervals $[t, t+\delta]$. Consider the previously defined expressions for the generic unitary vector $\mathbf{c}$, the observability Gramian, as well as for the function $\mathbf{f}(t,\tau)$ and its derivatives, noting that they all have bounded norm.

The sufficiency proof follows by exhaustion, showing that

$$\exists_{\substack{\delta>0 \\ \alpha>0}} \ \forall_{t\geq t_0} \ \forall_{\substack{\mathbf{c}\in\mathbb{R}^{n_c} \\ \|\mathbf{c}\|=1}} \ : \mathbf{c}^T \boldsymbol{\mathcal{W}}(t, t+\delta)\, \mathbf{c} \geq \alpha. \tag{12}$$

To do so, all the possibilities for the components of $\mathbf{c}$ are addressed, either establishing that $\|\mathbf{f}(t,\tau)\| \geq \alpha_1^*$ or $\left\|\frac{\partial}{\partial\tau}\mathbf{f}(t,\tau)\right\| \geq \alpha_2^*$ for every possible case, for some $\alpha_1^* > 0$, $\alpha_2^* > 0$, and $\tau \in \mathcal{T}_\delta$. Then, noting that Proposition 5 can be used, condition (12) is implied.

First, considering that $\|\mathbf{c}_M\| \geq \alpha_M$, for some $1 \geq \alpha_M > 0$, it can be seen that $\|\mathbf{f}(t,t)\| = \|\mathbf{c}_M\| \geq \alpha_M$, for all $t \geq t_0$, which implies (12). Now, consider the converse case where $\|\mathbf{c}_M\| < \alpha_M$, noting that this implies that $\|\mathbf{c}_V\| \geq \alpha_V$ for some $1 \geq \alpha_V > 0$, as $\|\mathbf{c}\| = 1$. Defining the auxiliary function

$$\mathbf{f}_V(t,\tau) := \int_t^\tau \mathbf{T}_M(\sigma)\,\mathbf{F}(\sigma)\,d\sigma\,\mathbf{c}_V^*$$

with $\mathbf{c}_V^* := \frac{\mathbf{c}_V}{\|\mathbf{c}_V\|}$, such that $\mathbf{f}(t,\tau) = \mathbf{c}_M + \mathbf{f}_V(t,\tau)\|\mathbf{c}_V\|$, it can be seen that

$$\begin{aligned}\|\mathbf{f}(t,\tau)\| \ \geq \ & \max(\|\mathbf{c}_M\|, \|\mathbf{f}_V(t,\tau)\|\|\mathbf{c}_V\|) \\ & - \min(\|\mathbf{c}_M\|, \|\mathbf{f}_V(t,\tau)\|\|\mathbf{c}_V\|)\end{aligned}$$

for all $t \geq t_0$ and $\tau \in \mathcal{T}_\delta$. Assuming that $\|\mathbf{f}_V(t,t^*)\| \geq \alpha_{f_V}$ if $\|\mathbf{c}_V\| \geq \alpha_V$, for some $t^* \in \mathcal{T}_\delta$ and $\alpha_{f_V} > 0$, and choosing any $\alpha_M \leq \frac{\alpha_{f_V}\,\alpha_V}{2}$, it can be seen that

$$\begin{aligned}\|\mathbf{f}(t,t^*)\| &\geq \|\mathbf{f}_V(t,t^*)\|\|\mathbf{c}_V\| - \|\mathbf{c}_M\| \\ &\geq \alpha_{f_V}\,\alpha_V - \frac{\alpha_{f_V}\,\alpha_V}{2} \\ &\geq \frac{\alpha_{f_V}\,\alpha_V}{2}\end{aligned}$$

which also implies (12). Thus, it remains to prove that, whenever $\|\mathbf{c}_V\| \geq \alpha_V$, then there exists $t^* \in \mathcal{T}_\delta$ such that $\|\mathbf{f}_V(t,t^*)\| \geq \alpha_{f_V}$. Recalling Proposition 5 and noting that $\mathbf{f}_V(t,t) = \mathbf{0}$, it is sufficient to show that there exists some $\alpha_{f_V}^* > 0$ such that there exists $\tau \in \mathcal{T}_\delta$ for which $\|\frac{\partial\,\mathbf{f}_V(t,\tau)}{\partial\tau}\| \geq \alpha_{f_V}^*$. To this end, without loss of generality, consider that $\mathbf{c}_V^* = \mathbf{c}_V$ such that $\mathbf{f}_V(t,\tau) = \int_t^\tau \mathbf{T}_M(\sigma)\,\mathbf{F}(\sigma)\,d\sigma\,\mathbf{c}_V$. Computing the derivative of this function, it is possible to conclude that

$$\left\|\frac{\partial\,\mathbf{f}_V(t,\tau)}{\partial\tau}\right\|^2 = \sum_{i=1}^m \|\mathbf{F}_i(\tau)\,\mathbf{c}_V\|^2$$

which, considering conditions 1–3 of the theorem, results in

$$\left\|\frac{\partial \mathbf{f}_V(t,\tau)}{\partial \tau}\right\|^2 = \|\mathbf{S}\,\mathbf{y}_{p_1}(\tau)\,c_b - \mathbf{c}_v\|^2 + \|\mathbf{S}\,\mathbf{y}_{p_2}(\tau)\,c_b - \mathbf{c}_v\|^2$$

$$\left\|\frac{\partial \mathbf{f}_V(t,\tau)}{\partial \tau}\right\|^2 = \|\mathbf{S}\,\mathbf{y}_{p_1}(\tau)\,c_b - \mathbf{c}_v\|^2 + \|\mathbf{S}\,\mathbf{y}_{d_1}(\tau)\,c_b\|^2$$

and

$$\left\|\frac{\partial \mathbf{f}_V(t,\tau)}{\partial \tau}\right\|^2 = \|\mathbf{S}\,\mathbf{y}_{p_1}(\tau)\,c_b - \mathbf{c}_v\|^2 = \left\|\mathbf{S}\,\mathbf{y}_{p_1}(t)\,c_b - \mathbf{c}_v + \mathbf{S}\int_t^\tau \dot{\mathbf{y}}_{p_1}(\sigma)\,d\sigma\,c_b\right\|^2$$

respectively, noting that

$$\mathbf{y}_{p_1}(\tau) = \mathbf{y}_{p_1}(t) + \int_t^\tau \dot{\mathbf{y}}_{p_1}(\sigma)\,d\sigma. \tag{13}$$

Using the reverse triangular inequality, it can be seen that

$$\begin{aligned}\|\mathbf{S}\,\mathbf{y}_{p_1}(\tau)\,c_b - \mathbf{c}_v\|^2 &\geq (\|\mathbf{S}\,\mathbf{y}_{p_1}(\tau)\,c_b\| - \|\mathbf{c}_v\|)^2\\ &= \|\mathbf{y}_{p_1}(\tau)\|^2\,|c_b|^2 + \|\mathbf{c}_v\|^2\\ &\quad - 2\,\|\mathbf{y}_{p_1}(\tau)\|\,|c_b|\,\|\mathbf{c}_v\|.\end{aligned}$$

Consider the case where $|c_b| < \alpha_b$, implying that $\|\mathbf{c}_v\| \geq \alpha_v$ for some $1 \geq \alpha_b > 0$ and $1 \geq \alpha_v > 0$, as $\|\mathbf{c}_V\| = 1$. Choosing $\alpha_b \leq \frac{\alpha_v}{4\,\bar{\alpha}_p}$, the previous equation becomes

$$\begin{aligned}\|\mathbf{S}\,\mathbf{y}_{p_1}(\tau)\,c_b - \mathbf{c}_v\|^2 &\geq \|\mathbf{c}_v\|\,(\|\mathbf{c}_v\| - 2\,\|\mathbf{y}_{p_1}(\tau)\|\,|c_b|)\\ &\geq \alpha_v\,(\alpha_v - 2\,\bar{\alpha}_p\,\alpha_b)\\ &\geq \frac{\alpha_v^2}{2}\end{aligned}$$

implying that $\|\frac{\partial \mathbf{f}_V(t,\tau)}{\partial \tau}\|^2 \geq \frac{\alpha_v^2}{2}$ for all the three conditions of the theorem. Considering the case where $\|\mathbf{c}_v\| < \alpha_v$, which also implies that $|c_b| \geq \alpha_b$, and choosing $\alpha_v \leq \frac{\alpha_{p_1}\,\alpha_b}{4}$, it can be seen that

$$\begin{aligned}\|\mathbf{S}\,\mathbf{y}_{p_1}(\tau)\,c_b - \mathbf{c}_v\|^2 &\geq \|\mathbf{y}_{p_1}(\tau)\|\,|c_b|\,(\|\mathbf{y}_{p_1}(\tau)\|\,|c_b| - 2\,\|\mathbf{c}_v\|)\\ &\geq \alpha_{p_1}\,\alpha_b\,(\alpha_{p_1}\,\alpha_b - 2\,\alpha_v)\\ &\geq \frac{\alpha_{p_1}^2\,\alpha_b^2}{2}\end{aligned}$$

which also implies that $\|\frac{\partial \mathbf{f}_V(t,\tau)}{\partial \tau}\|^2 \geq \frac{\alpha_{p_1}^2\,\alpha_b^2}{2}$ for all the three conditions of the theorem. The only remaining case is when both $\|\mathbf{c}_v\| \geq \alpha_v$ and $|c_b| \geq \alpha_b$, for which, if $\|\mathbf{S}\,\mathbf{y}_{p_1}(\tau)\,c_b - \mathbf{c}_v)\| \geq \alpha_1$ for some positive constant $\alpha_1 > 0$, then $\|\frac{\partial \mathbf{f}_V(t,\tau)}{\partial \tau}\| \geq \alpha_1$ for all the conditions 1–3 of the theorem, thus implying (12). Conversely, if $\|\mathbf{S}\,\mathbf{y}_{p_1}(\tau)\,c_b - \mathbf{c}_v)\| < \alpha_1$, the conditions of the theorem have to be addressed separately. For the first condition of the theorem, Assumption 2 implies that the two visible position landmarks are different and satisfy $\|\mathbf{y}_{p_1}(\tau) - \mathbf{y}_{p_2}(\tau)\| \geq \alpha_{p_{12}}$. It is a matter of algebraic manipulation to show that this relation can be rewritten as

$$\begin{aligned}\alpha_{p_{12}} &\leq \|\mathbf{y}_{p_1}(\tau) - \mathbf{y}_{p_2}(\tau)\|\\ \alpha_{p_{12}}\,\alpha_b &\leq \|\mathbf{S}\,\mathbf{y}_{p_1}(\tau)\,c_b - \mathbf{S}\,\mathbf{y}_{p_2}(\tau)\,c_b\|\\ \alpha_{p_{12}}\,\alpha_b &\leq \|(\mathbf{S}\,\mathbf{y}_{p_1}(\tau)\,c_b - \mathbf{c}_v) - (\mathbf{S}\,\mathbf{y}_{p_2}(\tau)\,c_b - \mathbf{c}_v)\|\\ \alpha_{p_{12}}\,\alpha_b &\leq \|\mathbf{S}\,\mathbf{y}_{p_1}(\tau)\,c_b - \mathbf{c}_v\| + \|\mathbf{S}\,\mathbf{y}_{p_2}(\tau)\,c_b - \mathbf{c}_v\|.\end{aligned}$$

Then, by choosing $\alpha_1 \leq \frac{\alpha_{p_{12}}\,\alpha_b}{2}$, it can be seen that

$$\begin{aligned}\|\mathbf{S}\,\mathbf{y}_{p_2}(\tau)\,c_b - \mathbf{c}_v\| &\geq \alpha_{p_{12}}\,\alpha_b - \alpha_1\\ &\geq \frac{\alpha_{p_{12}}\,\alpha_b}{2}\end{aligned}$$

which implies that $\|\frac{\partial \mathbf{f}_V(t,\tau)}{\partial \tau}\| \geq \frac{\alpha_{p_{12}}\,\alpha_b}{2}$. For the second condition of the theorem, considering $\alpha_1 \leq \frac{\alpha_{d_1}\,\alpha_b}{2}$, it is possible to show that

$$\begin{aligned}\left\|\frac{\partial \mathbf{f}_V(t,\tau)}{\partial \tau}\right\|^2 &= \|\mathbf{S}\,\mathbf{y}_{p_1}(\tau)\,c_b - \mathbf{c}_v\|^2 + \|\mathbf{y}_{d_1}(\tau)\|^2\,\|c_b\|^2\\ &\geq \|\mathbf{S}\,\mathbf{y}_{p_1}(\tau)\,c_b - \mathbf{c}_v\|^2 + \alpha_{d_1}^2\,\alpha_b^2\\ &\geq (\alpha_{d_1}\,\alpha_b - \|\mathbf{S}\,\mathbf{y}_{p_1}(\tau)\,c_b - \mathbf{c}_v\|)^2\\ &\geq (\alpha_{d_1}\,\alpha_b - \alpha_1)^2\\ &\geq \frac{\alpha_{d_1}^2\,\alpha_b^2}{4}.\end{aligned}$$

Finally, for the third condition of the theorem, the function $\int_t^\tau \dot{\mathbf{y}}_{p_1}(\sigma)\,d\sigma$ is zero for $\tau = t$ and that its derivative, which is simply given by $\dot{\mathbf{y}}_{p_1}(\tau)$, satisfies $\|\dot{\mathbf{y}}_{p_1}(t_1)\| \geq \alpha_{\dot{p}}$. Thus, using once again Proposition 5, it can be seen that there exists $t_2 \in \mathcal{T}_\delta$ and $\alpha_2 > 0$ such that $\|\int_t^{t_2} \dot{\mathbf{y}}_{p_1}(\sigma)\,d\sigma\| \geq \alpha_2$. Choosing $\alpha_1 \leq \frac{\alpha_2}{2}$, it can be seen that

$$\begin{aligned}&\left\|\frac{\partial \mathbf{f}_V(t,\tau)}{\partial \tau}\Big|_{\tau=t_2}\right\|\\ &= \left\|\mathbf{S}\,\mathbf{y}_{p_1}(t)\,c_b - \mathbf{c}_v + \mathbf{S}\int_t^{t_2} \dot{\mathbf{y}}_{p_1}(\sigma)\,d\sigma\,c_b\right\|\\ &\geq \left\|\mathbf{S}\int_t^{t_2} \dot{\mathbf{y}}_{p_1}(\sigma)\,d\sigma\,c_b\right\| - \|\mathbf{S}\,\mathbf{y}_{p_1}(t)\,c_b - \mathbf{c}_v\|\\ &\geq \alpha_2 - \alpha_1\\ &\geq \frac{\alpha_2}{2}.\end{aligned}$$

Therefore, for all $\|\mathbf{c}_V\| \geq \alpha_V$, the conditions of the theorem are sufficient to ensure that there exists $t^* \in \mathcal{T}_\delta$ such that $\|\mathbf{f}_V(t,t^*)\| \geq \alpha_{f_V}$. This concludes the proof for the sufficiency part of the theorem, for the pair $(\boldsymbol{\mathcal{A}}(t), \boldsymbol{\mathcal{C}}(t))$.

The proof of necessity is done by transposition, that is, we want to prove that if none of the conditions of the theorem are satisfied, then the pair $(\boldsymbol{\mathcal{A}}(t), \boldsymbol{\mathcal{C}}(t))$ is not UCB. This means that either no landmark is visible, clearly yielding unobservability, or the only visible position landmark satisfies

$$\forall_{\substack{\delta>0\\ \alpha_{\dot{p}}>0}}\ \exists_{t\geq t_0}\ \forall_{t^*\in\mathcal{T}_\delta}\ :\ \|\dot{\mathbf{y}}_{p_1}(t^*)\| < \alpha_{\dot{p}}.$$

For the latter case, consider that $\|\mathbf{c}_M\| = 0$, whereas $1 > \|\mathbf{c}_v\| \geq \alpha_v$ and $1 > |c_b| \geq \alpha_b$, for some $\alpha_b > 0$ and $\alpha_v > 0$. It is a matter of algebraic manipulation to show that

$$\begin{aligned}\mathbf{c}^T \boldsymbol{\mathcal{W}}(t,t+\delta)\,\mathbf{c} &= \int_t^{t+\delta} \|\mathbf{f}(t,\tau)\|^2\, d\tau \\ &= \int_t^{t+\delta} \left\| \int_t^{\tau} \mathbf{R}_g(\sigma_1)\left(\mathbf{S}\,\mathbf{y}_{p_1}(\sigma_1)\,c_b - \mathbf{c}_v\right) d\sigma_1 \right\|^2 d\tau \\ &\leq \int_t^{t+\delta} \left(\int_t^{\tau} \left\| \mathbf{S}\,\mathbf{y}_{p_1}(\sigma_1)\,c_b - \mathbf{c}_v \right\| d\sigma_1 \right)^2 d\tau\end{aligned}$$

which, using (13) and choosing $\mathbf{c}_v = \mathbf{S}\,\mathbf{y}_{p_1}(t)\,c_b$ and c_b such that $\|\mathbf{c}\| = 1$, yields

$$\begin{aligned}&\mathbf{c}^T \boldsymbol{\mathcal{W}}(t,t+\delta)\,\mathbf{c} \\ &\leq \int_t^{t+\delta} \left(\int_t^{\tau} \left\| \mathbf{S} \int_t^{\sigma_1} \dot{\mathbf{y}}_{p_1}(\sigma_2)\, d\sigma_2\, c_b \right\| d\sigma_1 \right)^2 d\tau \\ &\leq \int_t^{t+\delta} \left(\int_t^{\tau} \int_t^{\sigma_1} \|\dot{\mathbf{y}}_{p_1}(\sigma_2)\|\, d\sigma_2\, d\sigma_1\, |c_b| \right)^2 d\tau \\ &< |c_b|^2 \int_t^{t+\delta} \left(\int_t^{\tau} \int_t^{\sigma_1} \alpha_{\dot{p}}\, d\sigma_2\, d\sigma_1 \right)^2 d\tau \\ &< \frac{\alpha_{\dot{p}}^2}{2} \int_t^{t+\delta} (\tau - t)^4\, d\tau \\ &< \frac{\alpha_{\dot{p}}^2\, \delta^5}{10}.\end{aligned}$$

Considering $\alpha_{\dot{p}}^2 = \frac{10\,\epsilon}{\delta^5}$ with $\epsilon > 0$, it can be seen that

$$\forall_{\substack{\delta>0 \\ \epsilon>0}}\ \exists_{t\geq t_0}\ \forall_{\substack{\mathbf{c}\in\mathbb{R}^{n_c} \\ \|\mathbf{c}\|=1}} : \mathbf{c}^T \boldsymbol{\mathcal{W}}(t,t+\delta)\,\mathbf{c} < \epsilon$$

meaning that the pair $(\boldsymbol{\mathcal{A}}(t), \boldsymbol{\mathcal{C}}(t))$ is not UCB. Therefore, if the pair $(\boldsymbol{\mathcal{A}}(t), \boldsymbol{\mathcal{C}}(t))$ is UCB, the conditions of the theorem must hold. Noting that the Lyapunov transformation $\mathbf{T}(t)$ preserves observability properties, the uniform complete observability of the pair $(\mathbf{A}(t), \mathbf{C}(t))$ is achieved under the same conditions as for the pair $(\boldsymbol{\mathcal{A}}(t), \boldsymbol{\mathcal{C}}(t))$, which concludes the proof of the theorem. ■

ACKNOWLEDGMENT

The authors would like to thank the DSOR Lab Quadrotor team, particularly R. Cunha, B. Cardeira, D. Cabecinhas, A. Oliveira, P. Serra, and B. Gomes, for developing the ideal platform for data acquisition, which has enabled the experimental validation of the algorithm presented in this paper. The authors would also like to thank the editors and reviewers for their valuable comments and suggestions, which greatly improved the quality of the paper.

REFERENCES

[1] R. C. Smith and P. Cheeseman, "On the representation and estimation of spatial uncertainty," *Int. J. Robot. Res.*, vol. 5, no. 4, pp. 56–68, 1986.
[2] H. Durrant-Whyte, "Uncertain geometry in robotics," *IEEE J. Robot. Autom.*, vol. 4, no. 1, pp. 23–31, Feb. 1988.
[3] R. C. Smith, M. Self, and P. Cheeseman, *Estimating Uncertain Spatial Relationships in Robotics*. New York, NY, USA: Springer-Verlag, 1990, pp. 167–193.
[4] M. Csorba and H. Durrant-Whyte, "A new approach to simultaneous localisation and map building," presented at the *SPIE Aerosense*, Orlando, FL, USA, 1996.
[5] M. Csorba, "Simultaneous localisation and map building," Ph.D. dissertation, Univ. Oxford, Oxford, U.K., 1997.
[6] H. Durrant-Whyte and T. Bailey, "Simultaneous localization and mapping: Part I," *IEEE Robot. Autom. Mag.*, vol. 13, no. 2, pp. 99–110, Jun. 2006.
[7] T. Bailey and H. Durrant-Whyte, "Simultaneous localization and mapping (SLAM): Part II," *IEEE Robot. Autom. Mag.*, vol. 13, no. 3, pp. 108–117, Sep. 2006.
[8] S. Thrun, W. Burgard, and D. Fox, *Probabilistic Robotics*. Cambridge, MA, USA: MIT Press, 2005.
[9] J. Neira and J. Tardos, "Data association in stochastic mapping using the joint compatibility test," *IEEE Trans. Robot. Autom.*, vol. 17, no. 6, pp. 890–897, Dec. 2001.
[10] T. Bailey, "Mobile robot localisation and mapping in extensive outdoor environments," Ph.D. dissertation, Austral. Cent. Field Robotics, Univ. Sydney, NSW, Australia, 2002.
[11] G. Dissanayake, P. Newman, H. Durrant-Whyte, S. Clark, and M. Csobra, "A solution to the simultaneous localisation and mapping (SLAM) problem," *IEEE Trans. Robot. Autom.*, vol. 17, no. 3, pp. 229–241, Jun. 2001.
[12] S. Huang and G. Dissanayake, "Convergence and consistency analysis for extended Kalman Filter based SLAM," *IEEE Trans. Robot.*, vol. 23, no. 5, pp. 1036–1049, Oct. 2007.
[13] S. J. Julier and J. K. Uhlmann, "A counter example for the theory of simultaneous localization and map building," in *Proc. IEEE Int. Conf. Robot. Autom.*, May 2001, pp. 4238–4243.
[14] T. Bailey, J. Nieto, J. Guivant, M. Stevens, and E. Nebot, "Consistency of the EKF-SLAM algorithm," in *Proc. IEEE/RSJ Int. Conf. Intell. Robots Syst.*, Oct. 2006, pp. 3562–3568.
[15] J. Castellanos, J. Neira, and J. Tardos, "Limits to the consistency of EKF-based SLAM," presented at the *5th IFAC Symp. Intelligent Autonomous Vehicles*, Lisbon, Portugal, Jul. 2004.
[16] J. A. Castellanos, R. Martinez-Cantin, J. D. Tardos, and J. Neira, "Robocentric map joining: Improving the consistency of EKF-SLAM," *Robot. Auton. Syst.*, vol. 55, no. 1, pp. 21–29, Jan. 2007.
[17] G. Huang, A. Mourikis, and S. Roumeliotis, "A first-estimates Jacobian EKF for improving SLAM consistency," in *Experimental Robotics*, vol. 54, ser. Springer Tracts in Advanced Robotics, O. Khatib, V. Kumar, and G. Pappas, Eds.. Berlin, Germany: Springer-Verlag, 2009, pp. 373–382.
[18] A. N. Bishop and P. Jensfelt, "A stochastically stable solution to the problem of robocentric mapping," in *Proc. IEEE Int. Conf. Robot. Autom.*, May 2009, pp. 1615–1622.
[19] P. Batista, C. Silvestre, and P. Oliveira, "Optimal position and velocity navigation filters for autonomous vehicles," *Elsevier Automatica*, vol. 46, no. 4, pp. 767–774, Apr. 2010.
[20] P. Batista, C. Silvestre, and P. Oliveira, "On the observability of linear motion quantities in navigation systems," *Elsevier Syst. Control Lett.*, vol. 60, no. 2, pp. 101–110, Feb. 2011.
[21] P. Batista, C. Silvestre, and P. Oliveira, "Sensor-based globally asymptotically stable filters for attitude estimation: Analysis, design, and performance evaluation," *IEEE Trans. Autom. Control*, vol. 57, no. 8, pp. 2095–2100, Aug. 2012.
[22] B. J. Guerreiro, P. Batista, C. Silvestre, and P. Oliveira, "Sensor-based simultaneous localization and mapping—Part II: Online inertial map and trajectory estimation," in *Proc. Amer. Control Conf.*, Jun. 2012, pp. 6334–6339.
[23] B. J. Guerreiro, P. Batista, C. Silvestre, and P. Oliveira, "Sensor-based simultaneous localization and mapping—Part I: GAS robocentric filter," in *Proc. Amer. Control Conf.*, Jun. 2012, pp. 6352–6357.
[24] S. Bhat and D. Bernstein, "A topological obstruction to continuous global stabilization of rotational motion and the unwinding phenomenon," *Syst. Control Lett.*, vol. 39, no. 1, pp. 63–70, 2000.
[25] N. Chaturvedi, A. Sanyal, and N. McClamroch, "Rigid-body attitude control," *IEEE Control Syst.*, vol. 31, no. 3, pp. 30–51, Jun. 2011.
[26] P. Batista, C. Silvestre, and P. Oliveira, "Partial attitude and rate gyro bias estimation: Observability analysis, filter design, and performance evaluation," *Int. J. Control*, vol. 84, no. 5, pp. 895–903, May 2011.
[27] P. Batista, C. Silvestre, and P. Oliveira, "Single range aided navigation and source localization: Observability and filter design," *Syst. Control Lett.*, vol. 60, no. 8, pp. 665–673, Aug. 2011.
[28] R. Brockett, *Finite Dimensional Linear Systems*. New York, NY, USA: Wiley, 1970.

[29] H. K. Khalil, *Nonlinear Systems*, 3rd ed. Englewood Cliffs, NJ, USA: Prentice-Hall, 2002.
[30] B. Anderson, "Stability properties of Kalman-Bucy filters," *J. Franklin Inst.*, vol. 291, no. 2, pp. 137–144, 1971.
[31] A. Jazwinski, *Stochastic Processes and Filtering Theory*. New York, NY, USA: Academic, 1970.
[32] D. Goshen-Meskin and I. Y. Bar-Itzhack, "Observability analysis of piecewise constant systems. I. Theory," *IEEE Trans. Aerosp. Electron. Syst.*, vol. 28, no. 4, pp. 1056–1067, Oct. 1992.
[33] R. Kalman and R. Bucy, "New results in linear filtering and prediction theory," *Trans. ASME—J. Basic Eng.*, vol. 83, no. 3, pp. 95–108, Mar. 1961.
[34] A. Gelb, *Applied Optimal Estimation*. Cambridge, MA, USA: MIT Press, May 1974.
[35] T. Pavlidis and S. Horowitz, "Segmentation of plane curves," *IEEE Trans. Comput.*, vol. C-23, no. 8, pp. 860–870, Aug. 1974.
[36] C. Fernández, V. Moreno, B. Curto, and J. A. Vicente, "Clustering and line detection in laser range measurements," *Robot. Auton. Syst.*, vol. 58, pp. 720–726, 2010.
[37] J. D. Tardos, J. Neira, P. M. Newman, and J. J. Leonard, "Robust mapping and localization in indoor environments using sonar data," *Int. J. Robot. Res.*, vol. 21, pp. 311–330, 2002.

Bruno J. N. Guerreiro (M'12) received the Licenciatura degree in electrical and computer engineering in 2004 from Instituto Superior Técnico (IST), Lisbon, Portugal, where he is currently working toward the Ph.D. degree in the same field and has been involved in several research and development projects regarding the use of autonomous vehicles for automatic infrastructure inspection.

His research interests include sensor-based navigation and control of autonomous vehicles, laser calibration methods, and model predictive control.

Pedro Batista (M'10) received the Licenciatura degree in electrical and computer engineering in 2005 and the Ph.D. degree in 2010, both from Instituto Superior Técnico (IST), Lisbon, Portugal.

From 2004 to 2006, he was a Monitor with the Department of Mathematics, IST, where he is currently an Invited Assistant Professor with the Department of Electrical and Computer Engineering. His research interests include sensor-based navigation and control of autonomous vehicles.

Dr. Batista has received the Diploma de Mérito twice during his graduation and his Ph.D. thesis was awarded the Best Robotics Ph.D. Thesis Award by the Portuguese Society of Robotics.

Carlos Silvestre (M'07) received the Licenciatura degree in electrical engineering in 1987, the M.Sc. degree in electrical engineering in 1991, the Ph.D. degree in control science in 2001, and the Habilitation degree in electrical engineering and computers in 2011, all from the Instituto Superior Técnico (IST), Lisbon, Portugal.

Since 2000, he has been with the Department of Electrical Engineering, IST, where he is currently an Associate Professor of control and robotics in leave. Since 2012, he has been an Associate Professor with the Department of Electrical and Computers Engineering of the Faculty of Science and Technology, University of Macau, Taipa, Macau. He has conducted research on the subjects of navigation guidance and control of air and underwater robots. His research interests include linear and nonlinear control theory, coordinated control of multiple vehicles, gain scheduled control, integrated design of guidance and control systems, inertial navigation systems, and mission control and real time architectures for complex autonomous systems with applications to unmanned air and underwater vehicles.

Paulo Oliveira (SM'12) received the Ph.D. degree in 2002 from the Instituto Superior Técnico (IST), Lisbon, Portugal.

He is currently an Associate Professor with the Department of Mechanical Engineering, IST, Lisbon, Portugal and a Researcher with the Institute for Systems and Robotics, Associated Laboratory for Robotics and Systems in Engineering and Science, Lisbon, Portugal. His research interests include Robotics and Autonomous Vehicles with special focus on the fields of sensor fusion, navigation, positioning, and estimation. He has participated in more than 15 Portuguese and European Research projects over the last 20 years.